



Performance evaluation of three bio-optical models in aerosol and ocean color joint retrievals

Neranga K. Hannadige¹, Peng-Wang Zhai¹, Meng Gao^{2,3}, Yongxiang Hu⁴, P. Jeremy Werdell², Kirk Knobelspiesse², and Brian Cairns⁵

¹Department of Physics, University of Maryland Baltimore County, 1000 Hilltop Circle, Baltimore, MD 21250, USA

²NASA Goddard Space Flight Center, Code 616, Greenbelt, MD 20771, USA

³Science Systems and Applications, Inc., Greenbelt, MD 20706, USA

⁴NASA Langley Research Center, 1 Nasa Dr, Hampton, VA 23666, USA

⁵NASA Goddard Institute for Space Studies, 2880 Broadway, New York, NY 10025, USA

Correspondence: Peng-Wang Zhai (pwzhai@umbc.edu)

Received: 6 July 2023 – Discussion started: 25 July 2023

Revised: 30 September 2023 – Accepted: 6 October 2023 – Published: 1 December 2023

Abstract. Multi-angle polarimeters (MAPs) are powerful instruments to perform remote sensing of the environment. Joint retrieval algorithms of aerosols and ocean color have been developed to extract the rich information content of MAPs. These are optimization algorithms that fit the sensor measurements with forward models, which include radiative transfer simulations of the coupled atmosphere and ocean systems (CAOSs). The forward model consists of sub-models to represent the optics of the atmosphere, ocean water surface and ocean body. The representativeness of these models for observed scenes and the number of retrieval parameters are important for retrieval success. In this study, we have evaluated the impact of three different ocean bio-optical models with one, three and seven optimization parameters on the accuracy of joint retrieval algorithms of MAPs. The Multi-Angular Polarimetric Ocean coLor (MAPOL) joint retrieval algorithm was used to process data from the airborne Research Scanning Polarimeter (RSP) instrument acquired in different field campaigns. We performed ensemble retrievals along three RSP legs to evaluate the applicability of bio-optical models in geographically varying water of clear to turbid conditions. The average differences between the MAPOL aerosol optical depth (AOD) and spectral remote sensing reflectance ($R_{rs}(\lambda)$) retrievals and the MODerate resolution Imaging Spectroradiometer (MODIS) products were also reported. We studied the distribution of retrieval cost function values obtained for the three bio-optical models. For the one-parameter model, the spread of retrieval cost func-

tion values is narrow regardless of the type of water even if it fails to converge over coastal water. For the three- and seven-parameter models, the retrieval cost function distribution is water type dependent, showing the widest distribution over clear, open water. This suggests that caution should be used when using the spread of the cost function distribution to represent the retrieval uncertainty. We observed that the three- and seven-parameter models have similar MAP retrieval performances in all cases, though they are prone to converge at local minima over open-ocean water. It is necessary to develop a screening algorithm to divide open and coastal water before performing MAP retrievals. Given the computational efficiency and the algorithm stability requirements, we recommend the three-parameter bio-optical model as the coastal-water bio-optical model for future MAPOL studies. This study provides important practical guides on the joint retrieval algorithm development for current and future satellite missions such as NASA's Plankton, Aerosol, Cloud, ocean Ecosystem (PACE) mission and ESA's Meteorological Operational-Second Generation (MetOp-SG) mission.

1 Introduction

The enhanced capabilities in satellite remote sensing of Earth have enabled detailed observation of the atmosphere, ocean and land, thereby improving the accurate determination of spatial and temporal distributions of the con-

stituents of each. Satellite-borne spectroradiometers in particular have substantially advanced the way we view our home planet, and their information content will increase in the future as the technology evolves from multispectral to hyperspectral capabilities. Multi-angle polarimeters (MAPs), such as the Polarization and Directionality of the Earth's Reflectance (POLDER) (Deschamps et al., 1994), Airborne Multi-angle Spectro-Polarimetric Imager (AirMSPI) (Diner et al., 2013), Spectro-polarimeter for Planetary EXploration (SPEX) (Smit et al., 2019), Research Scanning Polarimeter (RSP) (Cairns et al., 2003), Multi-viewing Multi-Channel Multi-Polarization Imager (3MI) (Fougnie et al., 2018) and Multi-Angle Imager for Aerosols (MAIA) (Van Harten et al., 2021), have even greater information content compared to other existing single-viewing angle spectroradiometers, such as the MODerate Resolution Imaging Spectrometer (MODIS), Visible Infrared Imaging Radiometer Suite (VIIRS), and Ocean and Land Color Instrument (OLCI), owing to their ability to perform measurements at multiple viewing angles and different polarimetric states (Dubovik et al., 2019).

Atmospheric aerosols play a critical role in the Earth's climate and air quality (Boucher et al., 2013; Li et al., 2017). Aerosols affect Earth's energy balance directly by absorbing and scattering solar radiation and indirectly by interacting with clouds. Some of the traditional retrieval algorithms such as those for MODIS-like instruments result in larger aerosol and ocean color retrieval uncertainties when compared with the accuracy required for climate modeling (Remer et al., 2005; Sayer et al., 2016), which is due to the limited information content in single-viewing spectrometer measurements (Mishchenko et al., 2004). The large retrieval uncertainties of aerosols and ocean color also limit the accuracy of aerosol radiative forcing determination, thereby hindering our understanding of global climate change (Boucher et al., 2013). Improved aerosol characterization and quantification will support accurate estimation of atmospheric path radiance in the atmospheric correction (AC) process of ocean color remote sensing (Mobley et al., 2016). The spectral remote sensing reflectance ($R_{rs}(\lambda)$ (sr^{-1})) estimated through the AC process can be used to infer ocean optical and biogeochemical properties that are important for a broader understanding of phytoplankton dynamics, primary production, the global carbon cycle and the ocean's ecological response to climate change (Frouin et al., 2019).

AC is the process of removing atmospheric and surface contributions from the total measured signal at the top of the atmosphere (TOA) so that ocean color can be assessed. AC algorithms can be divided into two categories of processing strategies: traditional (or heritage) AC algorithms applicable to MODIS-like spectroradiometers (Gordon and Wang, 1994) and joint aerosol and ocean retrieval algorithms applicable to MAP measurements (Mishchenko and Travis, 1997; Chowdhary et al., 2001; Hasekamp and Landgraf, 2007; Knobelspiesse et al., 2012; Remer et al., 2019a, b). Tradi-

tional or heritage AC algorithms (Gordon and Wang, 1994) estimate the aerosol properties at near-infrared (NIR) wavelengths by assuming the water leaving radiance in NIR to be negligible or appropriately modeled (the so-called black pixel assumption) (Bailey et al., 2010). The aerosol properties are then extrapolated into the visible by using the appropriate aerosol models that fit NIR radiances (Zibordi et al., 2009; Gordon, 2021; Utry et al., 2014). This assumption does not unequivocally work in optically complex water, which can lead to an overestimate of aerosol path radiance either with nonzero NIR water leaving radiance or when absorbing aerosols are present (IOCCG, 2000, 2010). The heritage algorithm implemented by NASA's Ocean Biology Processing Group (OBPG; <https://oceancolor.gsfc.nasa.gov>, last access: 5 October 2023) works well over open water but can produce negative $R_{rs}(\lambda)$ in blue wavelengths over turbid water (Bailey et al., 2010) given the aforementioned reasons. Efforts have been made to overcome negative $R_{rs}(\lambda)$ (Bailey et al., 2010; He et al., 2012; Fan et al., 2021; Ibrahim et al., 2019), though the problem has not been fully resolved yet.

The second category of AC algorithms makes use of the larger information content available from MAPs. These instruments have a greater information content, which can be used to characterize aerosol microphysical properties (Mishchenko and Travis, 1997; Chowdhary et al., 2001; Hasekamp and Landgraf, 2007; Knobelspiesse et al., 2012; Remer et al., 2019a, b) and thus offer the potential for improvements in both aerosol and ocean color retrievals. Joint retrieval algorithms provide simultaneous retrievals of aerosols and ocean color by fitting the sensor measurements with forward model simulations for the coupled atmosphere and ocean system (CAOS) (Chowdhary et al., 2005; Hasekamp et al., 2011; Xu et al., 2016; Stamnes et al., 2018; Gao et al., 2018, 2019, 2020, 2021; Fan et al., 2021). The simulations are carried out by vector radiative transfer models with parameterizations that define the state of the CAOS. The difference between measurements and the model simulation is quantified by a cost function, which is minimized by iteratively perturbing the free parameters in the radiative transfer model. The forward model of ocean color joint retrieval algorithms consists of sub-models to simulate the optics of the CAOS, which is composed of the atmosphere, ocean surface and ocean body. The robustness of the joint retrieval algorithms depends on the representativeness of CAOS models over an observed scene. One important component of CAOS is the ocean bio-optical models that represent the spectral behaviors of aquatic inherent optical properties (IOP(λ s)) (e.g., pure seawater, phytoplankton, colored dissolved organic matter (CDOM) and non-algal particles (NAPs)) (IOCCG, 2006).

Ocean water is loosely classified into two categories, Cases I and II, based on the constituents present in the water and those constituents' relationships with $R_{rs}(\lambda)$. In Case I water the IOP(λ s) co-vary with the presence of phytoplankton and its derived CDOM, which are typically found off-

shore in the open ocean. The $IOP(\lambda)$ s of Case I water are typically parameterized using the concentration of the phytoplankton pigment chlorophyll *a* ([Chl *a*] [mg m^{-3}]) and, hence, result in single-parameter bio-optical models. Unlike Case I water, Case II water, which is most commonly found in coastal and turbid environments, consists of phytoplankton, NAP and CDOM, none of which are ubiquitously co-varied. Consequently, multiple parameters are required to represent Case II water $IOP(\lambda)$ s. Many joint retrieval algorithms (Chowdhary et al., 2005; Hasekamp et al., 2011; Xu et al., 2016; Stamnes et al., 2018) assume single-parameter bio-optical models developed for Case I water, whereas only a few algorithms (Chowdhary et al., 2012; Gao et al., 2018, 2019; Fan et al., 2021) adopt multi-parameter (three to seven parameters) bio-optical models. The choice of the bio-optical model has a great impact on the retrieval performance of joint retrieval algorithms. Fan et al. (2021) have studied the impact of different bio-optical models on retrieval accuracy, but their results were limited to radiometric measurements under a single-view angle. Gao et al. (2019) showed that a seven-parameter bio-optical model is superior in representing coastal water to the single-parameter model, though it is still an open question for the optimal bio-optical model for coastal water for joint retrieval algorithms.

The goal of this study is to examine the overall impact of bio-optical models with different numbers of free parameters on the performance and uncertainty of joint retrieval algorithms for Case II water. Hannadige et al. (2023) showed that multi-parameter bio-optical models with three and five parameters show similar retrieval performances for the semi-analytical algorithm (SAA) based on in situ multi-band $R_{rs}(\lambda)$ measurements. An independent study showed that the number of free parameters a retrieval algorithm might meaningfully retrieve is roughly four based on in situ hyperspectral $R_{rs}(\lambda)$ measurements (Cael et al., 2023). Here, for the first time, we have examined to which extent these conclusions hold for the joint retrieval algorithms using airborne MAP measurements, which have not been studied before. The quality of the retrievals in this study is evaluated with respect to the magnitude of the retrieval cost function values, the distribution of retrieval cost function values (Sect. 3) from the ensemble retrievals and the sanity check with MODIS retrievals. We studied the uncertainty of the different bio-optical models based on the spread of ensemble retrieval cost function values, which is important to understand the impact of the bio-optical models on the convergence behavior of the non-linear least squares fitting algorithms. This has not been examined in previous studies. Given the inherent problems associated with MODIS retrievals over optically complex scenes, we consider the MODIS products merely a reference rather than a validation dataset.

In this study the Multi-Angular Polarimetric Ocean coLor (MAPOL) joint retrieval algorithm (Gao et al., 2018, 2019, 2020) is used to evaluate the performance of the ocean bio-optical models with different numbers of

free parameters. MAPOL is an optimization approach that retrieves aerosol microphysical properties (aerosol optical depth (AOD), single scattering albedo (SSA), size distribution and refractive index) and in-water properties ($R_{rs}(\lambda)$, [Chl *a*] and component $IOP(\lambda)$ s) simultaneously. Three bio-optical models are used, i.e., the single-parameter model for open-ocean water and two coastal bio-optical models with three and seven free parameters, respectively. The MAPOL algorithm was used to inverse the Research Scanning Polarimeter (RSP) measurements from two NASA airborne campaigns (Aerosol Characterization from Polarimeter and Lidar (ACEPOL) (<https://www-air.larc.nasa.gov/missions/acepol>, last access: 10 December 2022) (Knobelspiesse et al., 2020) and North Atlantic Aerosols and Marine Ecosystems Study (NAAMES) (<https://www-air.larc.nasa.gov/missions/naames>, last access: 10 December 2022) (Behrenfeld et al., 2019). The RSP measurements were selected such that the underlying water represents clear to turbid water conditions. The retrieval results were checked against the AOD product from MODIS and High Spectral Resolution Lidar (HSRL)-2 (Burton et al., 2013) and ocean color products ($R_{rs}(\lambda)$ and [Chl *a*]) from MODIS. The retrieval uncertainties have been evaluated with respect to the Glory uncertainty requirement for AOD (Mishchenko et al., 2004) and PACE uncertainty requirements for open-ocean $R_{rs}(\lambda)$ (Werdell et al., 2019).

The conclusions from this study can be used to provide recommendations for selecting suitable bio-optical models for joint retrieval algorithms over coastal water to improve their accuracy and computational efficiency. The larger parameter space required for Case II parameterizations leads to longer forward model simulation times or decreases in the likelihood of accurate retrieval convergence. Thus, the balance between the model fidelity and the parameter space is vital to improve retrievals and uncertainties. This study also expects one to improve the performance of the polynomial-based atmospheric correction (POLYAC) algorithm (Hannadige et al., 2021), which is an AC algorithm for hyperspectral single-view radiometers applied over optically complex scenes, such as over coastal water. POLYAC relies on collocated MAP retrievals from the MAPOL algorithm to estimate the hyperspectral path radiance to calculate hyperspectral $R_{rs}(\lambda)$, which is crucial for retrieving phytoplankton functional types (IOCCG, 2014). Though this study was carried out with MAPOL, the conclusions are equally applicable to other joint retrieval algorithms of aerosols and ocean color, which thus have greater impacts beyond MAPOL.

This paper is organized as follows. Section 2 reviews the data used in the study; Sect. 3 describes the MAPOL algorithm and the respective bio-optical models; Sect. 4 presents the methodology and the retrieval results along with an uncertainty assessment under three different scenes; Sect. 5 discusses the overall results; and, finally, Sect. 6 summarizes the conclusions.

2 Data

2.1 Airborne data

In this study, we used airborne RSP measurements acquired from the ACEPOL 2017 (<https://www-air.larc.nasa.gov/missions/acepol/index.html>, last access: 10 December 2022) (Knobelspiesse et al., 2020) and NAAMES 2015 (<https://www-air.larc.nasa.gov/missions/naames/index.html>, last access: 10 December 2022) (Behrenfeld et al., 2019) airborne field campaigns. The ACEPOL campaign was held from 19 October to 9 November 2017, covering California, Nevada, Arizona, New Mexico and the coastal Pacific Ocean. NAAMES 2015 was the first deployment of the NAAMES campaign conducted from 5 November to 2 December 2015 over the North Atlantic Ocean.

RSP is an along-track scanner, with 152 viewing angles within $\pm 60^\circ$. It has nine spectral channels spanning the visible to shortwave infrared (SWIR) with central wavelengths of each band located at 410, 470, 550, 670, 865, 960, 1590, 1880 and 2250 nm. RSP-1 and RSP-2 are two versions of the RSP instrument that differ in measurement uncertainty characterizations. RSP measurements over oceans have been used for aerosol and ocean color retrievals in multiple studies (Chowdhary et al., 2005, 2012; Stamnes et al., 2018; Gao et al., 2019, 2020) with promising performances. In the ACEPOL campaign, RSP-2 measurements were acquired with a relative radiometric characterization uncertainty of approximately 0.03 and polarimetric characterization uncertainty of about 0.002 in degree of linear polarization (DoLP), whereas in the NAAMES 2015 campaign RSP-1 measurements were acquired with radiometric (relative) and polarimetric characterization uncertainties of approximately 0.015 and 0.002, respectively. The instrument noise model for RSP is provided in Knobelspiesse et al. (2019).

We performed MAP retrievals across three RSP flight legs over selected open- and coastal-water regions. From the ACEPOL campaign, we selected a coastal leg across Monterey Bay, where the water was mostly clear offshore and turbid when closer to the coast. From the NAAMES campaign, we selected a coastal leg across Delaware Bay and an open-ocean leg offshore and outward from Delaware Bay. Each case has been named based on the campaign and the type of water present: ACEPOL-Mix, NAAMES-Coastal and NAAMES-Open. Gao et al. (2019) showed a single-pixel retrieval from the NAAMES-Coastal case inside Delaware Bay comparing the retrieval performances of one- and seven-parameter bio-optical models. The details of the three cases are summarized in Table 1 and Fig. 1. The three cases were selected based on the availability of RSP measurements in cloud-free conditions, the water turbidity of the location and the availability of desired MODIS retrieval products. The turbidity of the water was assumed based on MODIS [Chl *a*] retrievals (Hu et al., 2012).

RSP wavelength bands corresponding to water vapor absorption (960 and 1880 nm), as well as those wavelength bands with high noise (1590 and 2250 nm bands only for DoLP), were excluded from the retrieval. The viewing angles contaminated by Sun glint and clouds were excluded from the retrieval to reduce retrieval uncertainty. For each location of interest, five consecutive pixels along the RSP leg were averaged to achieve better measurement accuracy. The RSP legs with averaged pixels are shown in Fig. 1. For the ACEPOL and NAAMES campaigns, the size of each averaged pixel is approximately 1 and 0.5 km, respectively. The corresponding averaged measurements (reflectance and DoLP) were applied in the retrieval.

2.2 Validation data

The AOD from the ACEPOL campaign is validated against HSRL-2. Due to the lack of at-sea in situ validation data, we performed sanity checks of the retrieval results using MODIS AOD and $R_{rs}(\lambda)$ products. MODIS is a single-view angle multispectral imager on both the NASA Terra and Aqua satellite platforms. The MODIS-OC (ocean color) product (NASA Ocean Color Web, 2020; <https://oceancolor.gsfc.nasa.gov>, last access: 5 October 2023) is processed using the standard NASA AC algorithm (Mobley et al., 2016) developed based on the atmospheric correction algorithm (Gordon and Wang, 1994) as modified by Ahmad et al. (2010). We used level 2 ocean color (OC) products from the MODIS instrument on board the Aqua satellite (version 2022.0). It provides a spatial coverage of 1 km resolution at nadir. The OC products include $R_{rs}(\lambda)$ at 412, 443, 469, 488, 531, 547, 555, 645, 667 and 678 nm and [Chl *a*] via the Color Index-based Algorithm (CIA; Hu et al., 2012). We also obtained MODIS AOD at 869 nm and the Ångström exponent derived from the standard NASA Atmospheric Correction (AC) algorithm to estimate the spectral AOD at RSP wavelengths. The ACEPOL 2017 campaign flew the HSRL-2 along with RSP, with the former instrument also providing accurate data for AOD validation.

3 The MAPOL joint retrieval algorithm

The MAPOL joint retrieval algorithm simultaneously retrieves aerosol and ocean color properties from MAP measurements. It has been validated with synthetic RSP data (Gao et al., 2018) and real RSP (Gao et al., 2019; Hannadige et al., 2021) and SPEX airborne measurements (Gao et al., 2020; Hannadige et al., 2021).

3.1 Retrieval cost function

The algorithm minimizes the difference between the MAP measurements and forward model simulations for CAOS (Zhai et al., 2009, 2010). The forward model simulation is iteratively optimized (Levenberg–Marquardt non-linear least

Table 1. Summary of the datasets used in this study.

| RSP leg | ACEPOL-Mix | NAAMES-Coastal | NAAMES-Open |
|------------------------|-----------------|-----------------|-----------------|
| Date | 7 November 2017 | 4 November 2015 | 4 November 2015 |
| Number of pixels | 62 | 40 | 106 |
| UTC time range | 20:13–20:25 | 18:21–18:26 | 17:34–18:20 |
| Aircraft altitude | 20 km | 6.7 km | 6.8 km |
| Solar zenith angle | 53° | 59° | 55° |
| Relative azimuth angle | 75° | 110° | 75° |
| Scattering angle range | [105°, 132°] | [91°, 132°] | [93°, 133°] |

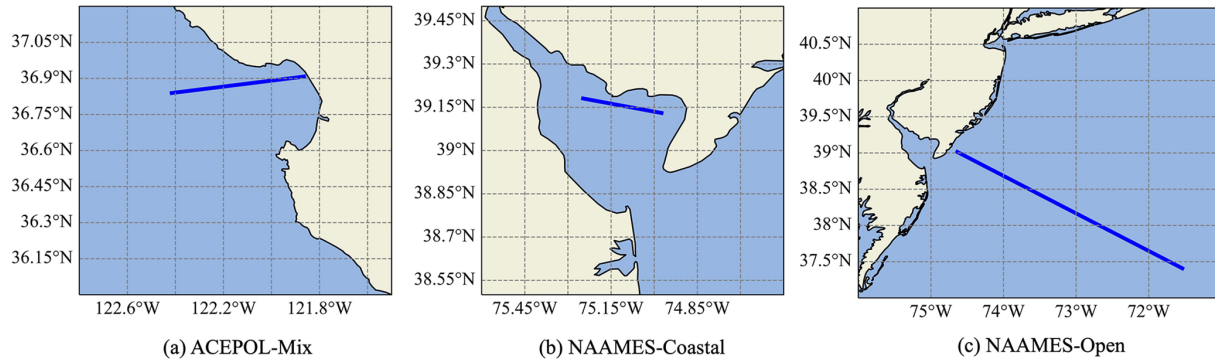


Figure 1. Geographical locations of the selected RSP legs.

squares optimization) by perturbing the set of free parameters that represent the atmosphere and ocean optical properties. The least squares cost function ($\chi^2(\mathbf{x})$) used to quantify the difference between the measurement and the forward model simulation is defined as

$$\chi^2(\mathbf{x}) = \frac{1}{N} \sum_i \left(\frac{[\rho_t(i) - \rho_t^f(\mathbf{x}; i)]^2}{\sigma_t^2(i)} + \frac{[P_t(i) - P_t^f(\mathbf{x}; i)]^2}{\sigma_p^2(i)} \right), \quad (1)$$

where $\rho_t = \pi r^2 L_t / \mu_0 F_0$ is the total measured reflectance, and $P_t = \sqrt{Q_t^2 + U_t^2} / L_t$ is the total measured DoLP. L_t , Q_t and U_t are the first three Stokes parameters measured at sensor level; μ_0 is the cosine of the solar zenith angle; F_0 is the extraterrestrial solar irradiance; and r is the Sun–Earth distance in astronomical units. ρ_t^f and P_t^f denote the total reflectance and DoLP simulated from the forward model. \mathbf{x} is the state vector of the retrieval, i is the measurement index corresponding to a particular angle or wavelength, and N is the total number of measurements used in the retrieval. σ_t and σ_p are the total uncertainties of reflectance and DoLP, which include the RSP instrument characterization (Knobelspiesse et al., 2019), variance due to averaging nearby pixels and forward model uncertainties. The forward model uncertainty is estimated as 0.015 and 0.002 for the radiometric and polarimetric uncertainties, respectively (Gao et al., 2023). The uncertainty correlation between angles has been ignored (Knobelspiesse et al., 2012; Gao et al., 2023).

The χ^2 value of a converged retrieval indicates the goodness of fit of the retrieval. A χ^2 value substantially larger

than 1 suggests the insufficiency of the forward model to accurately represent a given set of MAP measurements. A χ^2 close to 1 implies that the difference between the measurement and the corresponding forward model simulation is within the uncertainty quantified by σ_t and σ_p . In this study, we used χ^2 values obtained under each retrieval to assess their retrieval quality and performances.

3.2 Forward model

The forward model of the MAPOL algorithm is a vector radiative transfer model based on the successive order of scattering method (Zhai et al., 2009, 2010). The CAOS is defined as three layers: a top molecular layer, a middle layer with mixed aerosols and molecules (2 km height), and an ocean layer bounded by a rough water surface (Cox and Munk, 1954). The aerosol size distribution is composed of five spherical aerosol sub-modes: three fine modes and two coarse modes, each with a log-normal distribution. The mean radius and variance are fixed (Gao et al., 2020). The complex refractive index spectra of the two aerosol modes are based on the principal component analysis (PCA) of datasets representing spectral refractive indices of water, dust-like, biomass burning, industrial, soot, sulfate, water-soluble (Shettle and Fenn, 1979) and sea salt aerosols (de Almeida et al., 1991). The refractive indices are approximated as $m(\lambda) = m_0 + \alpha_1 p_1(\lambda)$, where m_0 and α_1 are fitting parameters, and $p_1(\lambda)$ is the first order of the principal component.

In the MAPOL forward model, the analytical Fournier–Forand phase function (F_p) (Fournier and Forand, 1994) is used to represent the particulate scattering phase function. The F_p is determined by B_p (i.e., b_{bp}/b_p) (Mobley et al., 1993). The overall phase function of water is obtained by mixing F_p with that of a pure-water phase function, which is then multiplied by the normalized Mueller matrix derived from measurements (Voss and Fry, 1984; Kokhanovsky, 2003) to obtain the total Mueller matrix of water assuming invariant polarization properties (Zhai et al., 2017).

MAPOL retrieves the spectral aerosol refractive indices described by eight parameters (two (fine and coarse) modes \times two PCA \times two parts (real and imaginary)); aerosol volume densities (five parameters, one for each aerosol sub-mode); one parameter to represent the roughness of ocean surface, i.e., wind (characterized by isotropic Cox Munk model; Cox and Munk, 1954); and either one, three or seven parameters to represent water IOP(λ)s depending on the choice of bio-optical model in the retrieval.

Bio-optical models

MAPOL includes two ocean bio-optical models in the forward model to represent Case I and II water separately. The Case I water bio-optical model (“C1P1”) is a single-parameter model based on [Chl a], where the number following “P” stands for the number of free parameters in the model. The Case II (“C2P7”) model contains seven bio-optical parameters. In this study, we have included a third Case II water bio-optical model with three parameters (“C2P3”). A detailed description of the bio-optical models is given below.

C2P7 (Eqs. 2–5) is a coastal or Case II bio-optical model with seven parameters.

$$a_{ph}(\lambda) = A_{ph}(\lambda)[\text{Chl } a]^{E_{ph}(\lambda)}, \quad (2)$$

$$a_{dg}(\lambda) = a_{dg}(440) \exp[-S_{dg}(\lambda - 440)], \quad (3)$$

$$b_{bp}(\lambda) = b_{bp}(660) \left(\frac{\lambda}{660} \right)^{-S_{bp}}, \quad (4)$$

$$B_p(\lambda) = B_p(660) \left(\frac{\lambda}{660} \right)^{-S_{Bp}}, \quad (5)$$

where $a_{ph}(\lambda)$ (m^{-1}) is the absorption coefficient of phytoplankton parameterized in terms of [Chl a] using A_{ph} and E_{ph} spectral coefficients obtained from Bricaud et al. (1998), $a_{dg}(\lambda)$ (m^{-1}) is the spectral absorption coefficient of CDOM and NAP, $b_{bp}(\lambda)$ (m^{-1}) is the spectral backscattering coefficient of particulate matter, $B_p(\lambda)$ is the spectral backscattering fraction of particulate matter, S_{dg} (nm^{-1}) is the spectral exponential slope of $a_{dg}(\lambda)$ (in nm^{-1}), S_{bp} is the spectral slope of the power law function of $b_{bp}(\lambda)$, and S_{Bp} is the spectral slope of the power law function of $B_p(\lambda)$. The magnitudes of the spectral slopes S_{dg} , S_{bp} and S_{Bp} depend

on the composition and the size of the oceanic particles and therefore represent microphysical properties such as refractive index, effective radius and particle size distribution slope (Jonasz, 2007). The seven free parameters are [Chl a], $a_{dg}(440)$, $b_{bp}(660)$, $B_p(660)$, S_{dg} , S_{bp} and S_{Bp} where 440 and 660 represent reference wavelengths in nanometers (nm).

C2P3 is a three-parameter model simplified from the C2P7 model (Eqs. 2–5). To reduce the number of free parameters, we fixed the spectral slopes. S_{dg} typically varies between 0.01 and 0.02 nm^{-1} in natural water. Based on the in situ measurements over oceans (Roesler et al., 1989), most of the existing bio-optical models such as the default configuration for the generalized IOP (GIOP-DC) model (Werdell et al., 2013) adopt $S_{dg} = 0.018 \text{ nm}^{-1}$. It has been found that the particulate backscattering ratio from in situ measurements shows little or no spectral dependence, and the mean particulate backscattering ratio is 0.010 (Chami et al., 2005; Whitmire et al., 2007). We have fixed S_{Bp} at 0 and assumed a spectrally invariant backscattering fraction B_p of 0.01. S_{bp} typically varies between 0 and 2 from small to large particles (Werdell et al., 2013). S_{bp} was fixed at 0.3 in this study which was obtained by a sensitivity analysis carried out by Hannadige et al. (2023). We acknowledge that these fixed values could deviate under specific water conditions. The remaining free parameters of the model are [Chl a], $a_{dg}(440)$ and $b_{bp}(660)$.

C1P1 (Eqs. 6–10) is a [Chl a]-based single-parameter Case I water bio-optical model (Zhai et al., 2015, 2017). The absorption coefficient of phytoplankton $a_{ph}(\lambda)$ is the same as Eq. (2). The absorption $a_{dg}(\lambda)$ is given by Eq. (3) as in the C2P7 model, though S_{dg} is fixed at 0.018 nm^{-1} , and $a_{dg}(440)$ is specified by Eqs. (6) and (7) in terms of [Chl a] (IOCCG, 2006):

$$a_{dg}(440) = p_2 a_{ph}(440) \quad (6)$$

$$p_2 = 0.3 + \frac{5.7 \times 0.5 a_{ph}(440)}{0.02 + a_{ph}(440)}. \quad (7)$$

Similarly, $b_{bp}(\lambda)$ is also contributed to only by phytoplankton and is expressed in terms of [Chl a] (Huot et al., 2008).

$$b_{bp}(\lambda) = B_p \times b_p(\lambda), \quad (8)$$

where $b_p(\lambda)$ (m^{-1}) is the spectral scattering coefficient of particulate matter.

$$b_p(\lambda) = b_p(660) \left(\frac{\lambda}{660} \right)^{-S_p} \quad (9)$$

$$b_p(660) = 0.347[\text{Chl } a]^{0.766} \quad (10)$$

In Eq. (9), S_p is the spectral coefficient of b_p . For $0.02 < [\text{Chl } a] < 2 \text{ mg m}^{-3}$, $S_p = -0.5(\log_{10}[\text{Chl } a] - 0.3)$. For $[\text{Chl } a] > 2 \text{ mg m}^{-3}$, $S_p = 0$. B_p is assumed to be spectrally invariant and is described as $B_p = 0.002 + 0.01(0.50 -$

$0.25\log_{10}[\text{Chl } a]$). The three bio-optical models are summarized in Fig. 2.

4 Retrieval results

We performed retrievals with the MAPOL algorithm (Sect. 3) for the three cases (ACEPOL-Mix, NAAMES-Coastal and NAAMES-Open) described in Sect. 2. Separate retrievals were carried out using each bio-optical model (C2P7, C2P3 and C1P1 described in Sect. 3) for all the cases, regardless of the type of water they represent.

The final retrieval results are based on the ensemble retrieval technique (Gao et al., 2019, 2020). The technique can reduce the likelihood of convergence of the algorithm at local minima instead of the global minimum. The ensemble retrieval was carried out by performing 100 retrievals for each averaged RSP pixel. For each retrieval, the retrieval parameters are initialized with randomly generated initial values of each parameter, which are confined within a boundary as specified in Table 2 for bio-optical model parameters (Gao et al., 2018, 2019; Hannadige et al., 2023) and as in Gao et al. (2018) for atmospheric parameters.

The retrievals were sorted based on their χ^2 distribution, which is attributed to whether the ensemble of retrievals converged at the global minimum (narrow χ^2 distribution) or different local minima (broad χ^2 distribution). For each of the RSP pixels, we averaged 30 % (i.e., cumulative probability = 30 %) of the total retrievals to calculate the final retrieval results. We studied average retrievals from all three bio-optical models using different cumulative probabilities at a time. About 30 % cumulative probability yielded the lowest χ^2 and retrieval variability. The selection of cumulative probability of less than 30 % did not leave enough ensemble retrievals to estimate the average retrieval results (for the C1P1 model this number is about 70 %; to make it consistent across all three bio-optical models, 30 % was selected). It should be noted that all the converged retrievals under the three case studies yielded χ^2 larger than 0.3. The minimum and maximum χ^2 values within this 30 % are denoted as χ_{\min}^2 and χ_{\max}^2 , respectively. For all three cases, the selection of the first 30 % lowest χ^2 retrievals resulted in χ_{\max}^2 values which are about five points higher than the χ_{\min}^2 (that is $\chi_{\max}^2 \approx 5 + \chi_{\min}^2$). The choice of the cumulative probability or the χ_{\max}^2 depends on the accuracy requirement of the retrieval.

The resultant uncertainties of the retrieval parameters are determined as the standard deviation of the retrievals within χ_{\min}^2 and χ_{\max}^2 . The uncertainties are associated with different initial values in the optimization. Due to a large number of retrieval parameters and the non-linearity of the cost functions, the choice of the initial values often becomes important (Gao et al., 2020). Based on Gao et al. (2020) and Gao et al. (2023), the uncertainty derived from ensemble retrievals within the χ_{\min}^2 – χ_{\max}^2 range may not always be comparable to

the uncertainty calculated from the error propagation method (Knobelspiesse et al., 2012). The error propagation method directly relates the retrieval uncertainties to measurement uncertainties. The evaluation of uncertainties calculated from the error propagation method is subject to future study.

4.1 ACEPOL-Mix

The minimum retrieval cost function value χ_{\min}^2 is affected by the type of water present and the bio-optical model employed in the retrieval. For relatively clear water, where $1 < [\text{Chl } a] < 3 \text{ mg m}^{-3}$, the χ_{\min}^2 values obtained under all the three bio-optical models are similar ($2 < \chi_{\min}^2 < 3$). The average χ_{\min}^2 value within 30 % of the lowest χ^2 retrievals ($\chi_{\text{avg}30\%}^2$) is comparable to the χ_{\min}^2 (Fig. 3). For C2P3 and C2P7, $\chi_{\text{avg}30\%}^2 < 1.5 \times \chi_{\min}^2$. This suggests that the ensemble retrieval χ^2 values have a narrow spread attributed to the fact that most of the retrievals have reached their global minimum.

With increasing turbidity towards the coast, the χ_{\min}^2 values from C1P1 retrievals follow an increasing trend with increasing $[\text{Chl } a]$. Both the C2P3 and C2P7 models show similar χ_{\min}^2 values along the track, whose χ_{\min}^2 values (< 5) also tend to increase with increasing $[\text{Chl } a]$ but with less variability than that of C1P1 ($\chi_{\min}^2 > 5$). Larger χ_{\min}^2 indicates the inability of the forward model to accurately fit the MAP measurement. In other words, the C1P1 model is insufficient to fully represent the turbid water IOP(λ)s compared to the C2P3 and C2P7 bio-optical models.

We further validated the retrieval results and evaluated the retrieval uncertainties (Figs. 4 and 6) associated with each bio-optical model using AOD retrievals from HSRL-2 and MODIS. MODIS and HSRL-2 AOD (Fig. 5) were collocated with RSP within a maximum distance of around 1.7 and 0.5 km. There are no in situ $R_{\text{rs}}(\lambda)$ measurements available for validation for this scene. Instead, we compared $R_{\text{rs}}(\lambda)$ with collocated MODIS $R_{\text{rs}}(\lambda)$ collected within a maximum distance of 0.5 km. The time difference between MODIS and RSP measurements is roughly 1 h. The MODIS 412, 469, 555 and 667 nm ocean color bands were chosen to compare the corresponding RSP $R_{\text{rs}}(\lambda)$ at 410, 470, 550 and 670 nm bands. AOD from RSP was compared with the MODIS AOD based on the AC data product, a choice to ensure the consistency of ocean color and aerosol data products. In this case study, the AOD and $R_{\text{rs}}(\lambda)$ retrievals obtained by averaging 30 % of the lowest χ^2 cases were compared with those obtained for the χ_{\min}^2 case (the results are not shown here). The comparison of RSP-retrieved AOD at 532 nm with HSRL-2 and MODIS is given in Fig. 5. For clear visualization, the density of the pixels has been reduced in the plots. The vertical bars indicate the 1σ uncertainty.

Regardless of the selected bio-optical model or the turbidity of the water, all three models, C1P1, C2P3 and C2P7, show similar AOD values, suggesting that the bio-

| C2P7 (7 parameters) | C2P3 (3 parameters) |
|--|--|
| $a_{\text{ph}}(\lambda) = A_{\text{ph}}(\lambda)[\text{Chla}]^{E_{\text{ph}}(\lambda)}$ $a_{\text{dg}}(\lambda) = \mathbf{a_{dg}(440)} \exp[-\mathbf{S_{dg}}(\lambda - 440)]$ $b_{\text{bp}}(\lambda) = \mathbf{b_{bp}(660)} \left(\frac{\lambda}{660}\right)^{-S_{\text{bp}}}$ $B_{\text{p}}(\lambda) = \mathbf{B_{p}(660)} \left(\frac{\lambda}{660}\right)^{-S_{\text{Bp}}}$ | $a_{\text{ph}}(\lambda) = A_{\text{ph}}(\lambda)[\text{Chla}]^{E_{\text{ph}}(\lambda)}$ $a_{\text{dg}}(\lambda) = \mathbf{a_{dg}(440)} \exp[-0.018(\lambda - 440)]$ $b_{\text{bp}}(\lambda) = \mathbf{b_{bp}(660)} \left(\frac{\lambda}{660}\right)^{-0.3}$ $B_{\text{p}} = 0.01$ |
| C1P1 (1 parameter) | |
| $a_{\text{ph}}(\lambda) = A_{\text{ph}}(\lambda)[\text{Chla}]^{E_{\text{ph}}(\lambda)}$ $a_{\text{dg}}(\lambda) = a_{\text{dg}}(440, [\text{Chla}]) \exp[-0.018(\lambda - 440)]$ $b_{\text{bp}}(\lambda) = b_{\text{p}}(660, [\text{Chla}]) \left(\frac{\lambda}{660}\right)^{-S_{\text{bp}}([\text{Chla}])}$ $B_{\text{p}} = [0.02 + 0.01(0.5 - 0.25 \log_{10}[\text{Chla}])]$ | |

Figure 2. The summary of the MAPOL bio-optical models. The free parameters of each model are indicated in bold.

Table 2. The upper and lower boundaries of the bio-optical model parameters.

| Parameter | Model | Lower/upper boundaries |
|---|------------------|------------------------|
| [Chl <i>a</i>] (mg m ⁻³) | C1P1, C2P3, C2P7 | 0.001/30.0 |
| <i>a</i> _{dg} (440) (m ⁻¹) | C2P3, C2P7 | 0.001/2.5 |
| <i>S</i> _{dg} (nm ⁻¹) | C2P7 | 0.005/0.02 |
| <i>b</i> _{bp} (660) (m ⁻¹) | C2P3, C2P7 | 0.001/0.1 |
| <i>S</i> _{bp} | C2P7 | 0.001/2.5 |
| <i>B</i> _p (660) | C2P7 | 0.001/0.05 |
| <i>S</i> _{Bp} | C2P7 | -0.2/0.2 |

optical model does not substantially influence AOD retrievals (Fig. 4). Overall, the MODIS AOD agrees with the averaged MAPOL AOD within 1σ of the retrieval of all three bio-optical models, except at 410 nm, at which the MODIS AOD is slightly outside of the 1σ AOD uncertainty limits.

The AOD retrieved by HSRL-2 and MODIS at 532 nm is similar. Based on the AOD retrieval comparison with respect to HSRL-2 and MODIS at 532 nm (Fig. 5), the C2P3 model shows the overall best agreement among the three bio-optical models (Table 3). The differences between the HSRL-2, MODIS and RSP-retrieved AOD may be related to different sampling volumes, viewing geometries of the instruments and retrieval algorithms.

In the comparison of *R*_{rs}(λ) retrievals under the three bio-optical models (Fig. 6), MODIS shows negative *R*_{rs}(λ) values at shorter wavelengths (410 and 470 nm) over the one or two pixels closest to the coast around 121.95° W. The AOD values over these pixels are also much larger compared to MAPOL retrievals. This indicates that the MODIS AC algorithm has overestimated the aerosol signal over coastal water, thereby making *R*_{rs}(λ) negative. There are no negative *R*_{rs}(λ)

values found in the MAPOL retrievals. MODIS-estimated *R*_{rs}(λ) values are higher than those from MAPOL for relatively clear water at 410, 470 and 550 nm but agree well at 670 nm with *R*_{rs}(λ) values retrieved from the C2P3 and C2P7 models. The C1P1 model also agrees well at 670 nm but not when closer to the coast. For the MODIS, comparably larger *R*_{rs}(λ) values at shorter wavelengths can be explained by the comparably smaller AOD values at the respective wavelengths. A smaller difference in AOD can lead to a larger difference in *R*_{rs}(λ). The differences between MODIS products and MAPOL retrievals using the three bio-optical models are given in Table 3.

The corresponding retrieval uncertainties for AOD and *R*_{rs}(λ) are calculated as discussed in Sect. 4. The retrieved AOD values are similar across the three bio-optical models, but their AOD uncertainties differ due to the differences in their retrieval χ² distribution. C1P1 shows the lowest AOD and *R*_{rs}(λ) retrieval uncertainties. Yet, even though C1P1 shows smaller uncertainties compared to the other two models, the accuracy of the *R*_{rs}(λ) retrievals is not satisfactory for the two most nearshore pixels with respect to MODIS. The

Table 3. ACEPOL-Mix: the average relative differences ($\frac{1}{N} \sum \left[\frac{a_{\text{model}} - a_{\text{MODIS}}}{a_{\text{MODIS}}} \right]$ (%), where a is either AOD or $R_{rs}(\lambda)$, and N is the total number of retrieved pixels (sample size); $N = 62$) of AOD and $R_{rs}(\lambda)$ between MODIS and the three bio-optical models (C1P1, C2P3 and C2P7) at 410, 470, 550 and 670 nm. Negative $R_{rs}(\lambda)$ values from MODIS were excluded. The differences are based on 30 % averaged retrievals. The standard deviations of the relative differences are given inside the parentheses.

| | | 410 nm | 470 nm | 550 nm | 670 nm |
|-------------------|------|-------------|-------------|-------------|-------------|
| AOD | C1P1 | 16.3 (7.4) | 8.9 (6.1) | 5.5 (5.4) | 9.3 (6.5) |
| | C2P3 | 19.9 (10.1) | 12.1 (7.9) | 6.5 (6.1) | 6.4 (6.0) |
| | C2P7 | 15.6 (8.6) | 8.5 (6.7) | 5.1 (5.7) | 10.3 (6.1) |
| $R_{rs}(\lambda)$ | C1P1 | 60.7 (6.0) | 56.8 (4.7) | 39.1 (9.3) | 34.6 (11.0) |
| | C2P3 | 66.9 (6.9) | 61.9 (10.7) | 40.1 (15.0) | 14.9 (12.8) |
| | C2P7 | 58.4 (5.6) | 53.6 (9.8) | 30.2 (13.0) | 17.3 (15.7) |

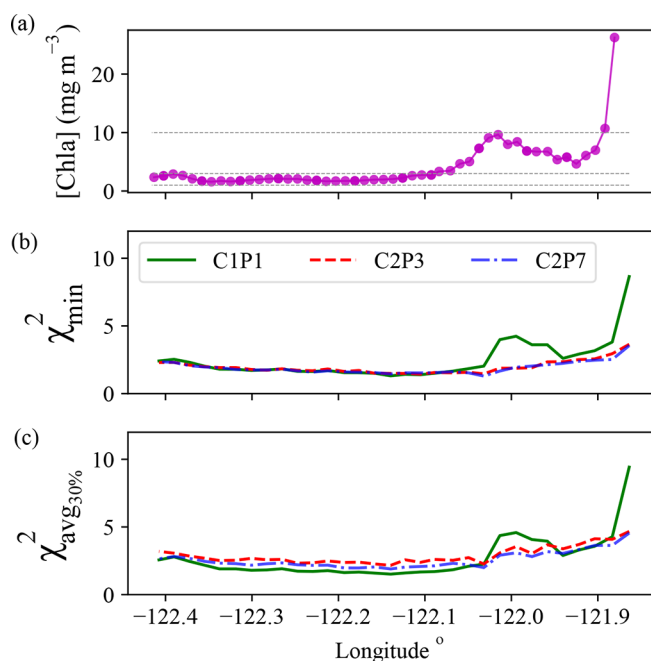


Figure 3. ACEPOL-Mix: panel (a) shows the MODIS-retrieved [Chl a]. The dashed gray lines indicate [Chl a] = 1, 3 and 10 mg m^{-3} . Panel (b) shows the χ^2_{min} obtained for the RSP retrievals across the ACEPOL-Mix leg under the three bio-optical models: C1P1, C2P3 and C2P7. Panel (c) shows the average χ^2_{min} value for the 30 % of the lowest χ^2 retrievals. Data are given with respect to the longitude of the location. The coast of Monterey Bay is to the right-hand side of the plots.

average uncertainty is less than 0.01 for AOD at all the given RSP wavelengths. This falls within the AOD uncertainty requirement defined by the Glory mission, namely a maximum of 0.02 over the ocean (Mishchenko et al., 2004). Overall, the C2P3 AOD uncertainty is slightly higher than that of C2P7. But it becomes smaller than that of C2P7 over the coastal water.

The $R_{rs}(\lambda)$ uncertainty values from C2P3- and C2P7-based retrievals are similar, with a maximum of 0.0004,

0.0005, 0.0007 and 0.0003 sr^{-1} at 410, 470, 550 and 670 nm, respectively. These uncertainties fall within the PACE-defined $R_{rs}(\lambda)$ uncertainty: from 400 to 600 nm the absolute uncertainty is 0.0006 sr^{-1} , and from 600 to 710 nm the absolute uncertainty is 0.0002 sr^{-1} (Werdell et al., 2019). For C1P1 the $R_{rs}(\lambda)$ uncertainty is less than 0.0002 sr^{-1} for all the wavelengths shown in Fig. 6 and falls within the PACE-defined $R_{rs}(\lambda)$ uncertainty.

The C1P1 AOD uncertainty is comparable with the other two models, but C1P1 $R_{rs}(\lambda)$ uncertainty is significantly lower than the other two models. One reason can be explained as the total number of free parameters in the retrieval. With the C1P1 model, there are a total of 15 parameters to be retrieved. For C2P3 and C2P7, that increases to 17 and 21, respectively. With fewer parameters, it is easier to converge at the global minimum within the parameter space, or a similar local minimum is always achieved. Here, for the C1P1 model, the majority of the retrievals are converged to the same point (either a local minimum or the global minimum); hence, the uncertainty defined by the spread of the cost function values is relatively small. With a larger number of free parameters in the retrieval, convergence can be achieved at a local minimum more often than at the global minimum. That makes the χ^2 distribution widespread; hence, the uncertainty becomes larger. Since C2P3 is a simplified version of the C2P7 model (that is a subset of the C2P7 model), we can expect C2P3 and C2P7 to have similar performances.

4.2 NAAMES-Coastal

The NAAMES-Coastal case (4 November 2015) covers RSP retrievals over Delaware Bay (Fig. 1b), which is a coastal-water region with high turbidity. The χ^2_{min} value obtained for each pixel with the three bio-optical models (C1P1, C2P7 and C2P3) is given at the bottom of Fig. 7. The averaged χ^2_{min} for the 30 % of the lowest χ^2 ($\chi^2_{\text{avg30\%}}$) cases is the same as χ^2_{min} for C1P1 and roughly twice the χ^2_{min} value for both C2P3 and C2P7. We did not see a significant difference between the retrieval results obtained from the lowest χ^2 case and 30 % average; hence, only the averaged AOD

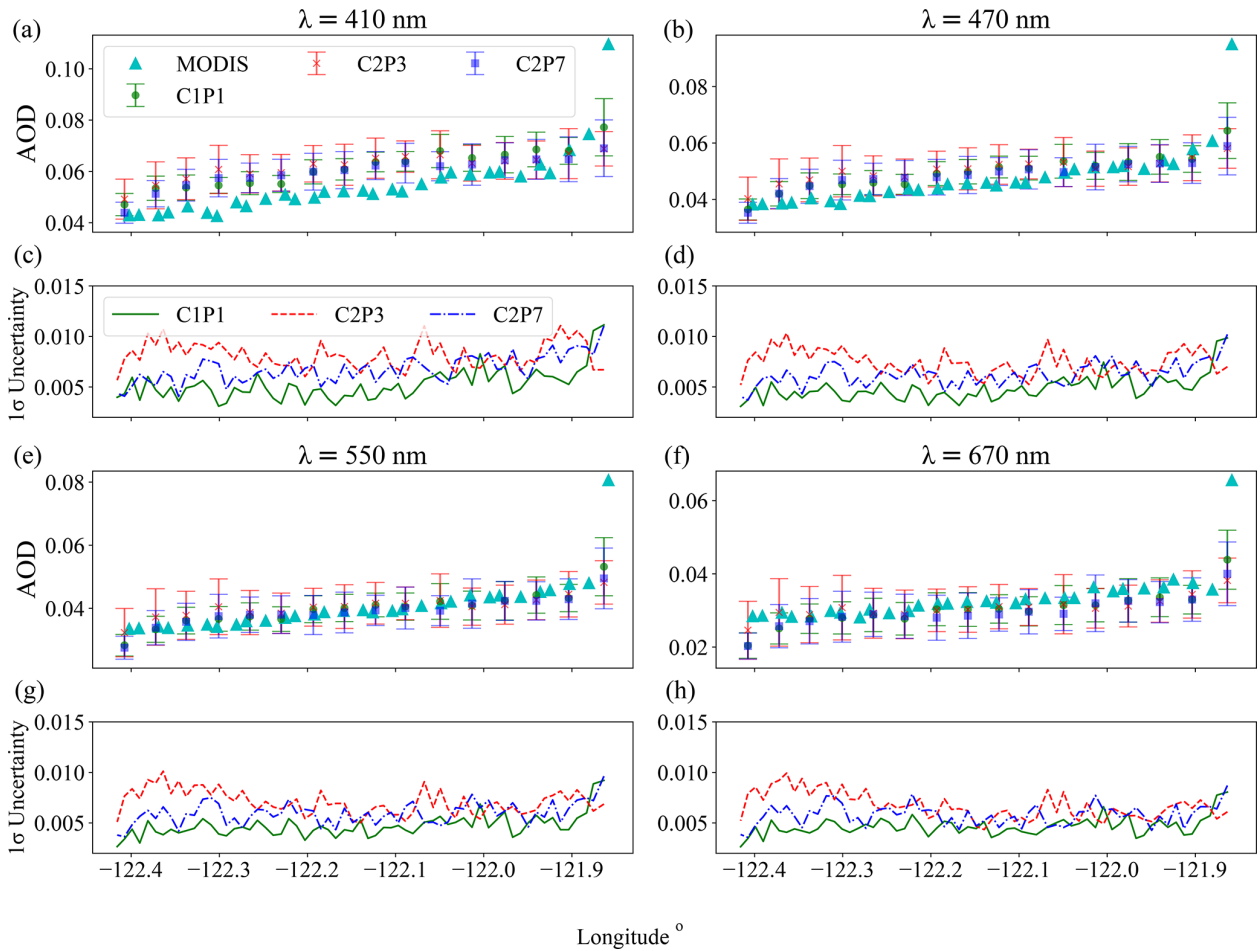


Figure 4. ACEPOL-Mix: the comparison of RSP-retrieved averaged spectral AOD across Monterey Bay with MODIS AOD and retrieval uncertainty. Results are shown for the retrievals under the three bio-optical models C1P1, C2P3 and C2P7 at 410, 470, 550 and 670 nm for averaged retrievals. The vertical bars indicate the 1σ uncertainty. Data are given with respect to the longitude of the location. The coast of Monterey Bay is to the right-hand side of the plots.

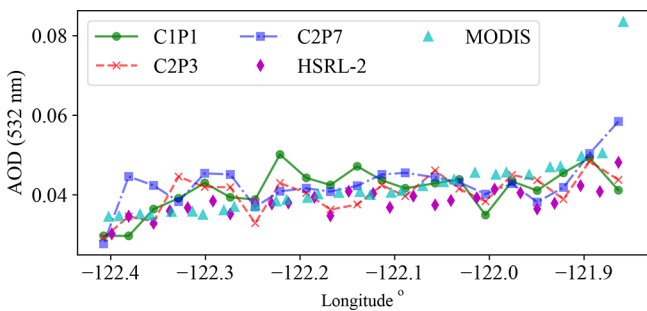


Figure 5. ACEPOL-Mix: the comparison of retrieved AOD at 532 nm with HSRL-2 and MODIS AOD at 532 nm. The AOD obtained for the lowest χ^2 case is shown here. Results are shown for the retrievals under the three bio-optical models C1P1, C2P3 and C2P7. Data are given with respect to the longitude of the location. The coast of Monterey Bay is to the right-hand side of the plots.

and $R_{rs}(\lambda)$ retrievals are shown here. The MODIS [Chl *a*] data (Fig. 7) show values larger than 5 mg m^{-3} , and the peak value exceeds 20 mg m^{-3} . The C1P1 model has shown the highest χ^2_{min} values around 100 still with a narrow χ^2 distribution, whereas both C2P3 and C2P7 models show χ^2_{min} values around 1.5. The large χ^2_{min} values around 100 with narrow χ^2 distributions imply the insufficiency of the C1P1 model to represent highly turbid coastal water. This also suggests that caution needs to be taken when using the cost function spread to study the uncertainty of retrieval parameters. Overall, the C2P3 and C2P7 models show the same capability to represent turbid coastal water.

The averaged AOD obtained under the C1P1 model is larger than that obtained with C2P3 and C2P7, likely because the C1P1 model misrepresents the water properly in Delaware Bay (Fig. 8). We collocated the MODIS AOD and ocean color products within a maximum distance of 0.8 km. The time difference between MODIS and RSP scan-

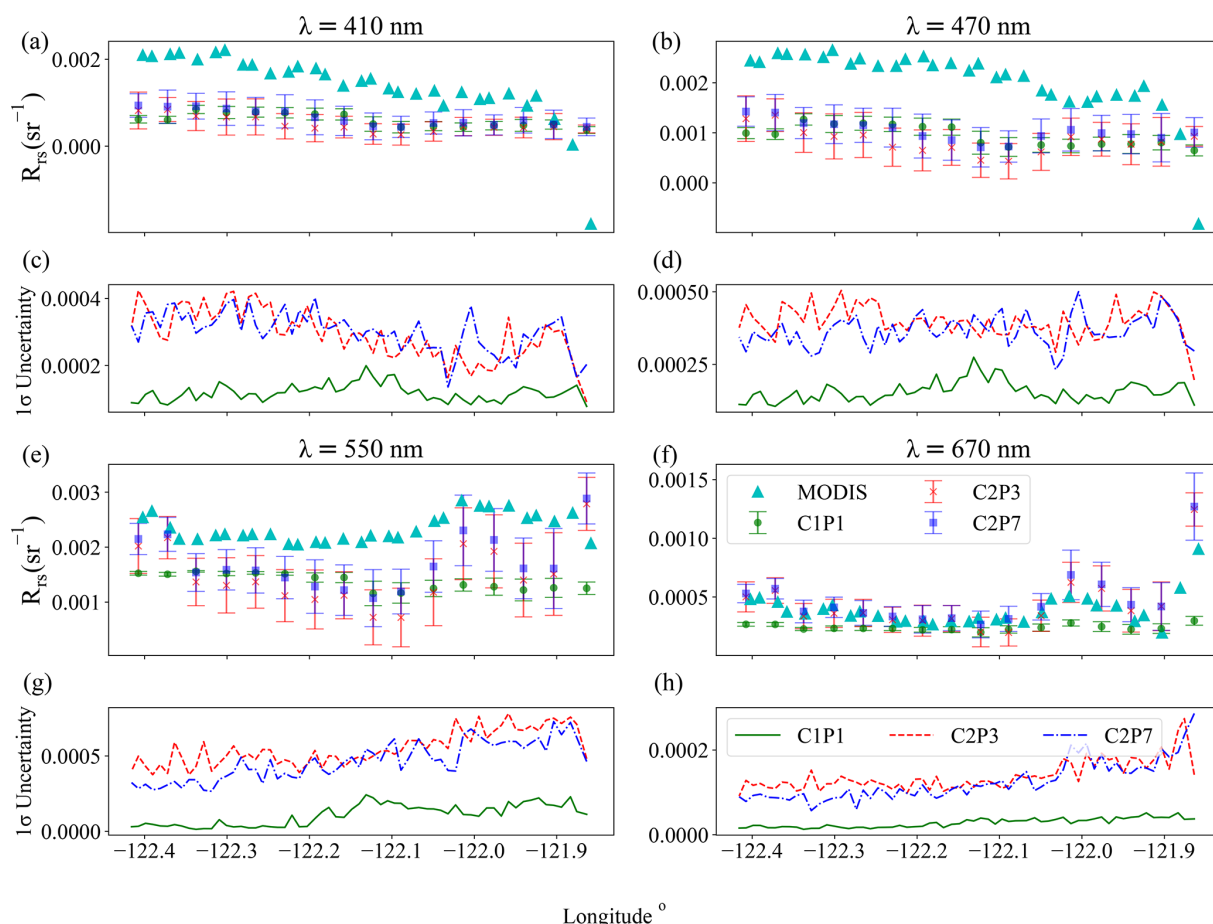


Figure 6. ACEPOL-Mix: the comparison of the RSP-retrieved averaged $R_{rs}(\lambda)$ across Monterey Bay with MODIS $R_{rs}(\lambda)$ product and retrieval uncertainty. Results are shown for the retrievals under the three bio-optical models C1P1, C2P3 and C2P7 at 410, 469, 554 and 670 nm for averaged retrievals. The vertical bars indicate the 1σ uncertainty. Data are given with respect to the longitude of the location. The coast of Monterey Bay is to the right-hand side of the plots.

ning times is approximately 1 h. The MODIS AOD values at 410 nm are within the uncertain limits of C1P1 and fall within the uncertainty limits of C2P3 and C2P7 at the rest of the wavelengths. Correspondingly, the C1P1 $R_{rs}(\lambda)$ is less than that from C2P3 and C2P7 (Fig. 9). At 410 and 470 nm, the $R_{rs}(\lambda)$ retrieved with C2P7 is on average larger than that from C2P3, but similar values are retrieved at 550 and 670 nm. The MODIS $R_{rs}(\lambda)$ agrees well with C2P3 and C2P7 at 470, 550 and 670 nm. At 410 nm, MODIS $R_{rs}(\lambda)$ is mostly similar to that retrieved from C2P3. The average relative differences between MODIS AOD and $R_{rs}(\lambda)$ with MAPOL retrievals under the three bio-optical models are given in Table 4.

The AOD and $R_{rs}(\lambda)$ retrieval uncertainties (Figs. 8 and 9) are generally similar across the three bio-optical models, with a few exceptions seen for C1P1 $R_{rs}(\lambda)$ uncertainty at longer wavelengths. The average AOD uncertainty is less than 0.02 at all the given RSP wavelengths and meets the AOD uncertainty requirement for climate models as assessed

by Mishchenko et al. (2004). The $R_{rs}(\lambda)$ uncertainty for the C2P7 model is larger at shorter wavelengths (410 and 470 nm), where the corresponding $R_{rs}(\lambda)$ signals are small. Overall, the C2P3 and C2P7 models result in $R_{rs}(\lambda)$ uncertainties near the uncertainty defined by the PACE mission except at 670 nm. Even though the $R_{rs}(\lambda)$ retrieval uncertainties are very small, the significantly larger χ^2 values under the C1P1 model and the inability to match the MODIS retrievals suggest that the C1P1 model is not suitable to represent the coastal-water properties.

4.3 NAAMES-Open

The NAAMES-Open case (4 November 2015) covers RSP retrievals along the open ocean outward from Delaware Bay (Fig. 1c). The χ_{\min}^2 values obtained for each pixel, under the three bio-optical models (C1P1, C2P7 and C2P3), are shown in Fig. 10b. The averaged χ_{\min}^2 for the 30 % of the lowest χ^2 cases is the same as χ_{\min}^2 for C1P1, and around 5 times the χ_{\min}^2 value for both C2P3 and C2P7, showing larger χ^2

Table 4. NAAMES-Coastal: the average relative differences (%) of AOD and $R_{rs}(\lambda)$ between MODIS and the three bio-optical models (C1P1, C2P3 and C2P7) at 410, 470, 550 and 670 nm. Sample size is $N = 40$. The differences are based on 30 % averaged retrievals. Negative $R_{rs}(\lambda)$ values from MODIS were excluded. The standard deviations of the relative differences are given inside the parentheses.

| | | 410 nm | 470 nm | 550 nm | 670 nm |
|-------------------|------|-------------|-------------|------------|------------|
| AOD | C1P1 | 9.7 (4.2) | 4.1 (2.9) | 11.7 (6.3) | 29.5 (9.9) |
| | C2P3 | 22.0 (3.5) | 12.5 (4.4) | 4.7 (3.7) | 13.8 (7.6) |
| | C2P7 | 23.6 (3.4) | 14.0 (4.5) | 5.4 (3.7) | 13.0 (7.3) |
| $R_{rs}(\lambda)$ | C1P1 | 31.4 (21.2) | 63.4 (10.2) | 75.5 (4.5) | 90.5 (1.7) |
| | C2P3 | 17.4 (14.7) | 18.4 (6.2) | 7.1 (4.3) | 7.6 (5.7) |
| | C2P7 | 60.8 (35.3) | 7.9 (4.5) | 10.5 (5.9) | 7.9 (4.8) |

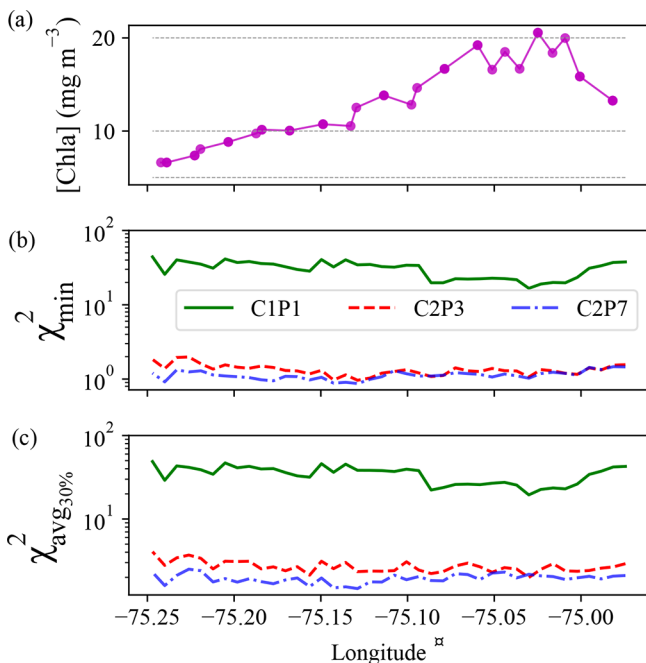


Figure 7. NAAMES-Coastal: panel (a) shows MODIS [Chl a]. The dashed gray lines indicate [Chl a] = 5, 10 and 20 mg m^{-3} . Panel (b) shows χ^2_{\min} obtained for the RSP retrievals under the three bio-optical models: C1P1, C2P3 and C2P7. Panel (c) shows the average χ^2_{\min} value for the 30 % of the lowest χ^2 retrievals. Data are given with respect to the longitude of the location. The RSP leg is located along the eastward coast of Delaware Bay.

distributions. This implies that the C2P3 and C2P7 models result in retrievals that converge at different local minima, instead of the global minimum. The MODIS [Chl a] values (Fig. 10a) are less than 0.5 mg m^{-3} in the open ocean and increase up to 4 mg m^{-3} closer to the coast/Delaware Bay. The χ^2_{\min} values are similar across all three bio-optical models with values around 1. There are some pixels from longitude 71.5 to 72.3° W which show larger χ^2_{\min} values, which we found to be attributed to cirrus cloud contamination.

For this case, we collocated MODIS AOD and $R_{rs}(\lambda)$ within a maximum distance of 1.4 and 0.5 km, respectively.

The time difference between MODIS and RSP scanning times is 1 h. The comparison with MODIS AOD (Fig. 11) shows a better agreement with averaged AOD retrievals from all three bio-optical models. Some exceptions are seen in the locations that were attributed to cloud contamination. Unlike the previous two cases, the C1P1-averaged $R_{rs}(\lambda)$ values show the best agreement with MODIS $R_{rs}(\lambda)$ values, mostly over open water (Fig. 12). The C2P3- and C2P7-averaged $R_{rs}(\lambda)$ values show better agreement only when closer to the coast (-74.5° W), where C1P1 is not expected to provide a complete representation of the water optical properties.

For the C2P3 and C2P7 models, the comparison of $R_{rs}(\lambda)$ retrievals obtained for the lowest χ^2 retrieval of the ensemble retrieval shows better agreement with MODIS $R_{rs}(\lambda)$ compared to the averaged retrievals. For AOD, the C2P3- and C2P7-averaged retrievals show a better agreement with MODIS AOD than the lowest χ^2 retrievals. However, the agreement of the lowest χ^2 AOD retrievals from C2P3 and C2P7 with MODIS is better than that from C1P1. The relative differences between MODIS- and MAPOL-retrieved AOD corresponding to χ^2_{\min} and $\chi^{\text{avg}30\%}$ are given in Table 5, and the same for $R_{rs}(\lambda)$ is given in Table 6. There is a significant difference seen in the relative difference values between χ^2_{\min} and $\chi^{\text{avg}30\%}$ for $R_{rs}(\lambda)$ which is not significant for AOD. The distribution of χ^2 values in the ensemble retrieval therefore largely affects the accuracy of $R_{rs}(\lambda)$ retrievals.

The AOD uncertainties (Fig. 11) are similar across the three bio-optical models, with a maximum of 0.015 at all given wavelengths. For $R_{rs}(\lambda)$ (Fig. 12) C1P1 shows the lowest uncertainties owing to its small parameter space, which leads to better convergence near the global minimum. The multi-parameter models show comparably larger $R_{rs}(\lambda)$ uncertainties that are still within the PACE-defined uncertainties except at 410 nm.

5 Discussion

In this study, we have evaluated the retrieval performances of three bio-optical models within CAOSs under different water conditions. For the ACEPOL-Mix case, the water varies from relatively clear to highly turbid conditions, with [Chl a]

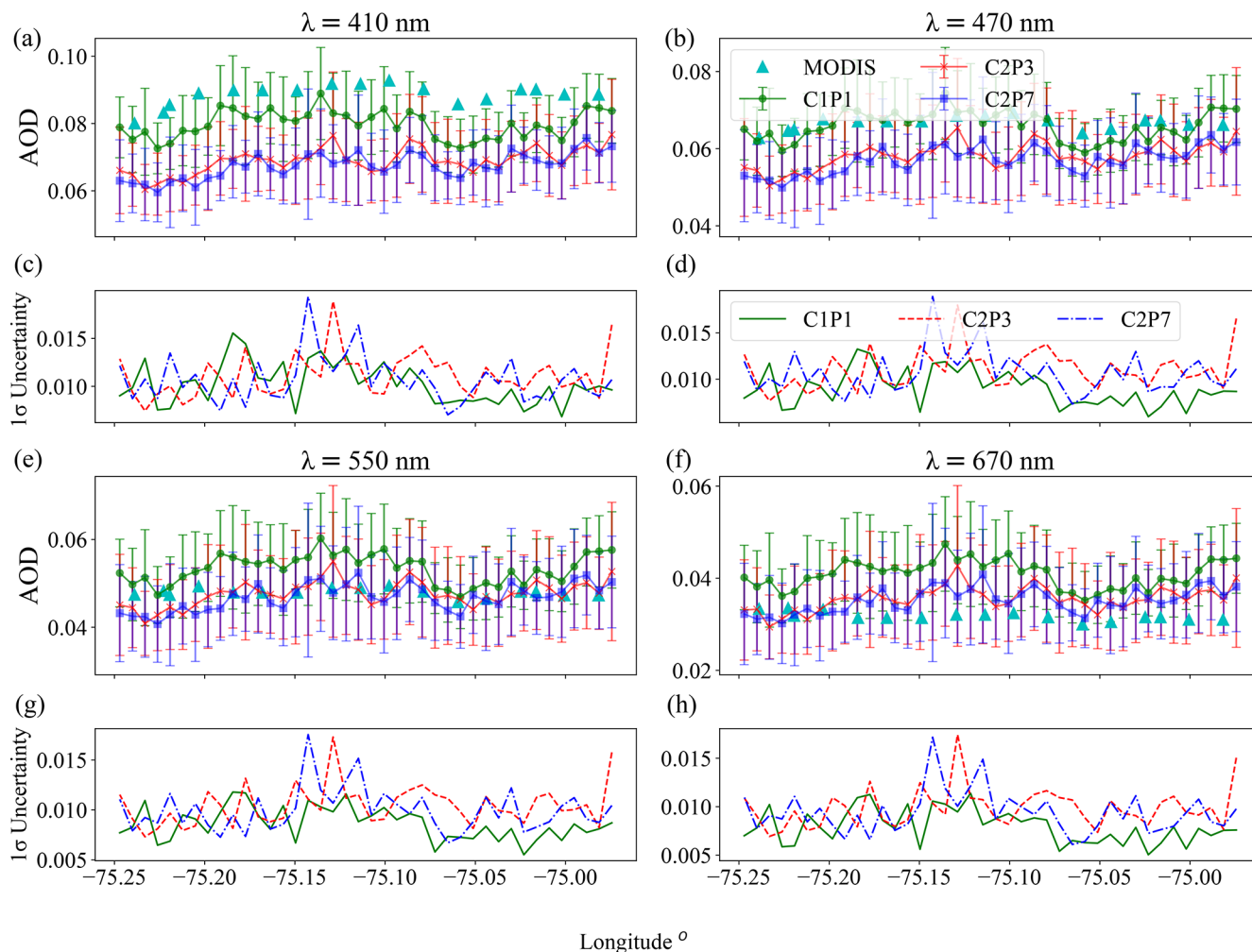


Figure 8. NAAMES-Coastal: the comparison of the RSP-retrieved averaged AOD across Delaware Bay with MODIS AOD and uncertainty. Results are shown for the retrievals under the three bio-optical models C1P1, C2P3 and C2P7 at 410, 470, 550 and 670 nm for averaged retrievals. The vertical bars indicate the 1σ uncertainty. Data are given with respect to the longitude of the location. The RSP leg is located along the eastward coast of Delaware Bay.

Table 5. NAAMES-Open: the average relative differences (%) of AOD between MODIS and the three bio-optical models (C1P1, C2P3 and C2P7) at 470, 550 and 670 nm. Sample size is $N = 106$. The differences are given for the retrievals from χ^2_{\min} case and averaged retrievals $\chi^2_{\text{avg}30\%}$. The standard deviation of the relative differences is given inside the parentheses.

| | | 410 nm | 470 nm | 550 nm | 670 nm |
|---------------------------|------|-------------|-------------|-------------|-------------|
| $\chi^2_{\text{avg}30\%}$ | C1P1 | 7.2 (4.7) | 9.0 (5.9) | 13.7 (9.0) | 20.7 (11.9) |
| | C2P3 | 9.0 (6.0) | 8.6 (5.2) | 13.5 (8.4) | 21.6 (11.6) |
| | C2P7 | 7.4 (5.1) | 7.9 (5.0) | 13.3 (8.4) | 21.6 (13.0) |
| χ^2_{\min} | C1P1 | 19.7 (12.0) | 25.5 (13.3) | 31.4 (16.5) | 40.5 (23.0) |
| | C2P3 | 31.3 (10.7) | 36.7 (11.2) | 44.9 (13.2) | 53.5 (15.7) |
| | C2P7 | 29.0 (11.7) | 34.3 (12.2) | 45.5 (13.7) | 51.1 (16.2) |

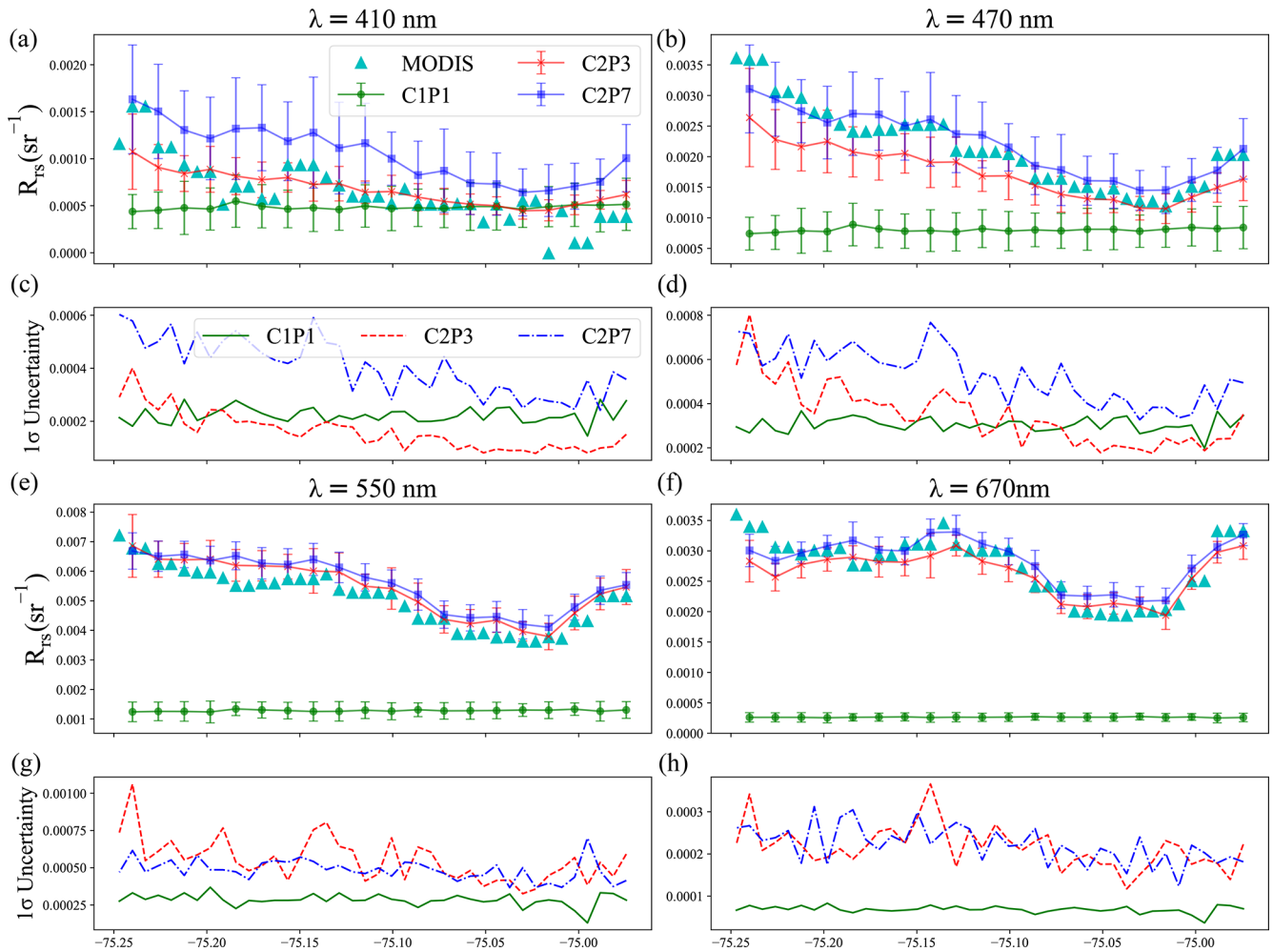


Figure 9. NAAMES-Coastal: the comparison of the RSP-retrieved averaged $R_{rs}(\lambda)$ across Delaware Bay with MODIS $R_{rs}(\lambda)$ product and uncertainty. Results are shown for the retrievals under the three bio-optical models C1P1, C2P3 and C2P7 at 410, 470, 550 and 670 nm for averaged retrievals. The vertical bars indicate the 1σ uncertainty. Data are given with respect to the longitude of the location. The RSP leg is located along the eastward coast of Delaware Bay.

Table 6. The same as Table 5 but for $R_{rs}(\lambda)$.

| | | 410 nm | 470 nm | 550 nm | 670 nm |
|---------------------------|------|-------------|-------------|-------------|-------------|
| $\chi^2_{\text{avg}30\%}$ | C1P1 | 27.0 (16.6) | 25.7 (11.4) | 21.0 (8.9) | 19.2 (6.1) |
| | C2P3 | 84.0 (7.3) | 84.4 (8.4) | 69.0 (10.6) | 52.5 (10.7) |
| | C2P7 | 80.0 (10.4) | 81.8 (10.6) | 67.2 (12.9) | 49.7 (13.2) |
| χ^2_{min} | C1P1 | 20.6 (16.4) | 20.9 (11.4) | 21.5 (9.0) | 51.0 (6.6) |
| | C2P3 | 27.2 (22.7) | 42.8 (15.7) | 24.8 (16.6) | 36.8 (15.6) |
| | C2P7 | 22.3 (20.3) | 37.7 (15.2) | 21.3 (16.4) | 33.2 (16.9) |

values ranging from 1–20 mg m^{-3} . The NAAMES-Coastal case includes RSP measurements over highly turbid water ($5 < [\text{Chl } a] < 20 \text{ mg m}^{-3}$). For the NAAMES-Open case, the water is mostly clear and becomes turbid when closer to the coast ($0.1 < [\text{Chl } a] < 3 \text{ mg m}^{-3}$).

We have evaluated the retrieval performances based on the magnitude of the retrieval cost function values, the spread of the cost function distribution, the validity of the retrieved AOD and $R_{rs}(\lambda)$ values, and the corresponding retrieval uncertainties. For the NAAMES-Open case, the C1P1 model shows low χ^2_{min} values, indicating good fitting against RSP

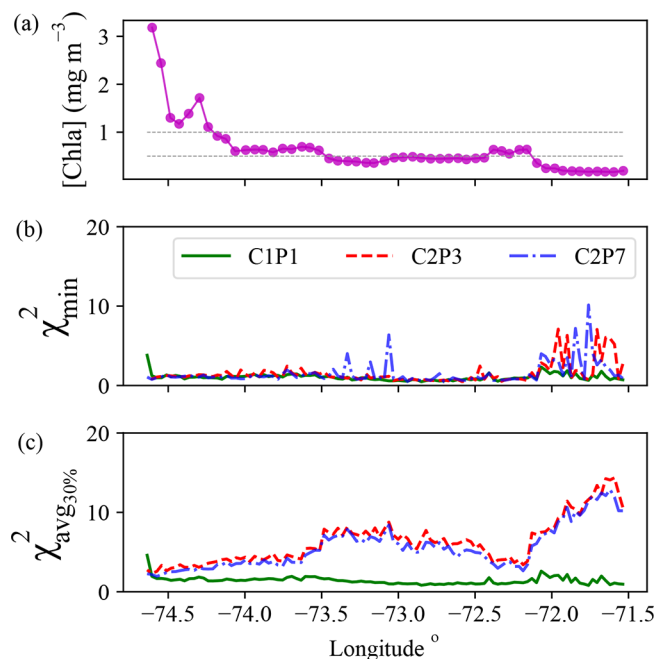


Figure 10. NAAMES-Open: panel (a) shows MODIS [Chl a]. The dashed gray lines indicate [Chl a] = 0.5 and 1 mg m^{-3} . Panel (b) shows χ^2_{\min} obtained for the RSP retrievals under the three bio-optical models: C1P1, C2P3 and C2P7. Panel (c) shows the average χ^2_{\min} value for the 30% of the lowest χ^2 retrievals. Data are given with respect to the longitude of the location. The coast is to the left-hand side of the plots.

measurements. The C2P3 and C2P7 models also show good fitting with the RSP measurements but only when the χ^2_{\min} cases are considered. The C1P1 model shows the best agreement in AOD and $R_{rs}(\lambda)$ retrieval results with independent data sources from the MODIS. The C1P1 retrieval performance in the ACEPOL-Mix case is satisfactory when the water is relatively clear ([Chl a] < 3 mg m^{-3}), that is, towards the open ocean. The C2P3 and C2P7 models in the NAAMES-Coastal case and nearshore ACEPOL-Mix pixels show better agreement in averaged AOD and $R_{rs}(\lambda)$ retrievals with uncertainties within the Glory uncertainty requirement for AOD and the PACE uncertainty requirement for $R_{rs}(\lambda)$.

The overall results indicate that the choice of bio-optical model (either a single parameter or multi-parameter) affects the accuracy of the retrievals, which is especially true for $R_{rs}(\lambda)$ retrievals. Hannadige et al. (2023) showed similar retrieval performances for three- and five-parameter bio-optical models when $R_{rs}(\lambda)$ is inverted using SAA-based algorithms. Here we demonstrated that the joint retrieval performances of the C2P3 and C2P7 models are mostly similar, showing that the same conclusion holds for joint retrieval algorithms using the airborne MAP measurements. For coastal water, it is inappropriate to use the single-parameter bio-optical

model. The C2P3 and C2P7 models show good retrieval performances over turbid water.

We have also evaluated the distribution of ensemble χ^2 values based on χ^2_{\min} and $\chi^2_{\text{avg}30\%}$ values. The study of cost function distributions helps us understand the impact of bio-optical models on the convergence behavior of the non-linear least squares fitting algorithms. For the C1P1 model, the χ^2 distribution from all three cases is narrow, and even the resultant χ^2 values are large. This suggests that the use of cost function distribution alone to study the uncertainty of retrieval parameters is misleading. For C2P3 and C2P7, over moderately to highly turbid water (ACEPOL-Mix and NAAMES-Coastal, $1 < [\text{Chl } a] < 20 \text{ mg m}^{-3}$), the χ^2 values are mostly closer to 1, and the distribution is nearly narrow, implying their capability to reach near the global minimum with multiple parameters over coastal water. But in the NAAMES-Open case, C2P3 and C2P7 show widespread χ^2 distributions, implying their inability to reach the global minimum with multiple parameters over open water. This can be explained by the degrees of freedom in the water leaving signal and the number of optimization parameters in the bio-optical models.

In the NAAMES-Open case, even though the averaged retrieval results from C2P3 and C2P7 are on average not satisfactory over clear water, the retrieval results corresponding to the lowest χ^2 show good agreement with MODIS AOD and $R_{rs}(\lambda)$. This implies that the C2P3 and C2P7 models can accurately represent clear water optical properties with proper interpretation and conscientious use of the χ^2 distributions. However, the averaged retrieval results differ significantly, as the retrieval χ^2 distributions under the C2P3 and C2P7 models are widespread compared to that of C1P1. For the practical use of these bio-optical models, we suggest performing initial retrievals using the C1P1 bio-optical model and then re-performing the retrievals with either C2P3 or C2P7 models in case the C1P1 model results in significantly larger χ^2 values.

The C2P3 and C2P7 models show similar retrieval performances for all three case studies. The MAPOL retrievals under the C2P3 model use 17 retrieval parameters, whereas the C2P7 model uses 21 parameters. The C2P7 provides a larger parameter space that encompasses all the possible parameter value combinations of the C2P3 model; hence, their performances are similar. MAPOL is computationally demanding, as it needs to iteratively run the radiative transfer forward model for CAOS. The algorithm stability and the time taken for a single retrieval are proportional to the size of the retrieval parameters. For the C2P3 model, it takes an average of 3 h for a single CPU core to process one-pixel retrieval with RSP measurements, whereas for the C2P7 model the time increases up to 8 h, since an increased number of parameters leads to more forward model and Jacobian evaluations in least squares fitting algorithms. Therefore, the C2P3 model is more efficient for the MAPOL algorithm to represent Case II water.

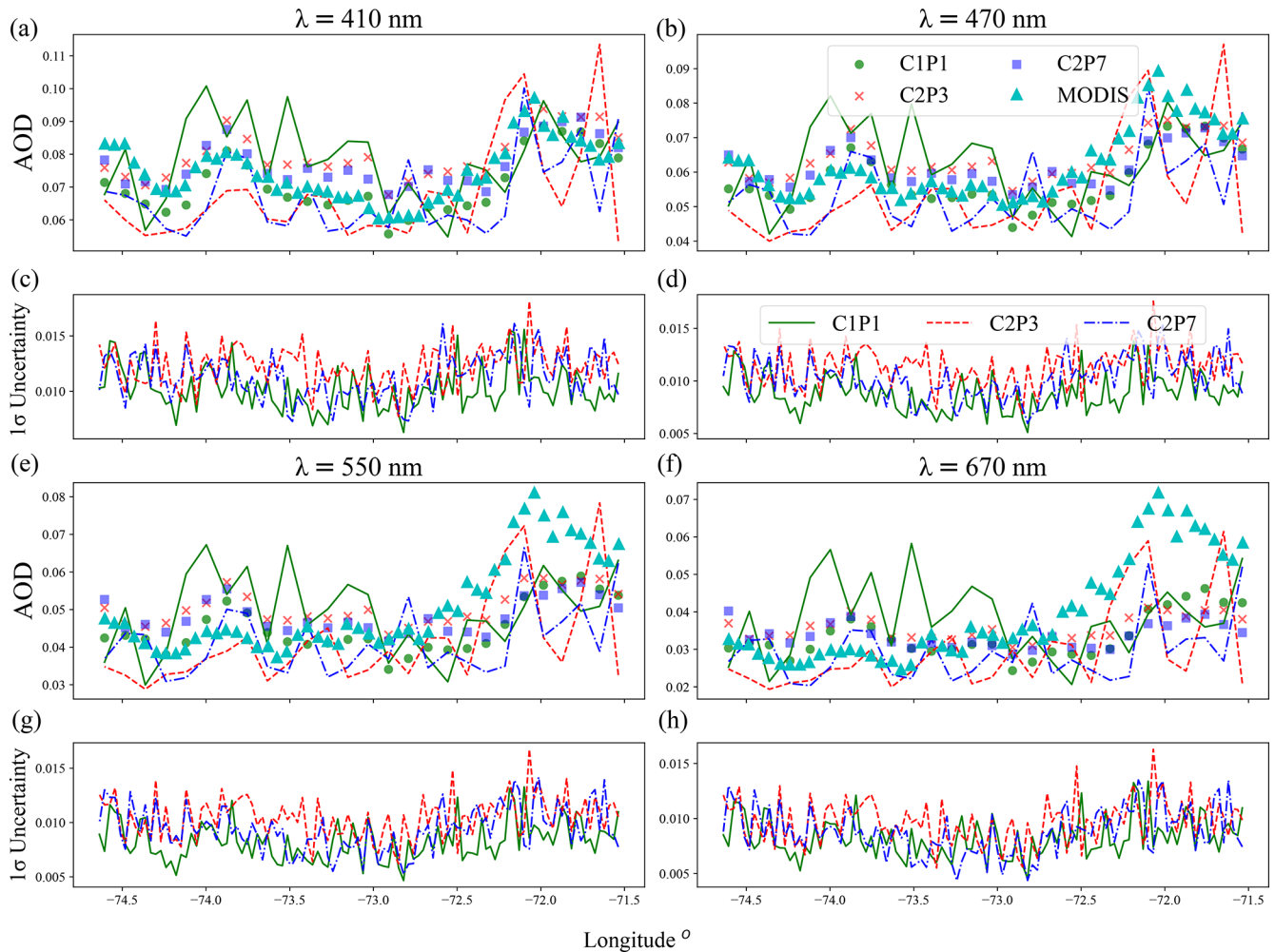


Figure 11. NAAMES-Open: the comparison of the RSP-retrieved spectral AOD across the open ocean with MODIS AOD and uncertainty. Results are shown for the retrievals under the three bio-optical models C1P1, C2P3 and C2P7 at 410, 469, 554 and 670 nm for averaged retrievals. The lines (C1P1 – solid, C2P3 – dashed, C2P7 – dotted) indicate the retrievals obtained for the χ_{\min}^2 case. The markers show the average retrieval. The uncertainty plots show the 1σ uncertainty for averaged retrievals. Data are given with respect to the longitude of the location. The coast is to the left-hand side of the plots.

The operational version of MAPOL, called FastMAPOL, replaces the radiative transfer forward model with neural networks, which can process several pixels within a second in a single CPU (Gao et al., 2021). We expect to update both the MAPOL and FastMAPOL algorithms with the C2P3 model in the future. The fixed parameters in the three-parameter C2P3 model might not be true for all the water, which is subject to fine-tuning. The availability of airborne MAP measurements over the oceans under cloud-free conditions is limited, and we cannot cover a larger range of atmosphere and water conditions in this study. The unavailability of accurate in situ measurements over the selected locations for the validation is yet another limitation. We expect to further improve our bio-optical models based on the MAP measurements to be acquired from the PACE mission plan to launch in early 2024.

The [Chl *a*] alone does not fully represent the turbidity of the water, as the sediment/NAP concentration and CDOM availability are also important factors. There is no clear boundary between Case I and II water (IOCCG, 2000); hence, we cannot provide a clear set of conditions where we need to apply each of the bio-optical models used in this study. There is no universal bio-optical model to represent water bio-optical properties (Fan et al., 2021). At least two separate bio-optical models are required to represent Case I and II water. The three cases in this study do not cover inland/lake water. The applicability of C2P3 and C2P7 to lakes or inland water is subject to a future study.

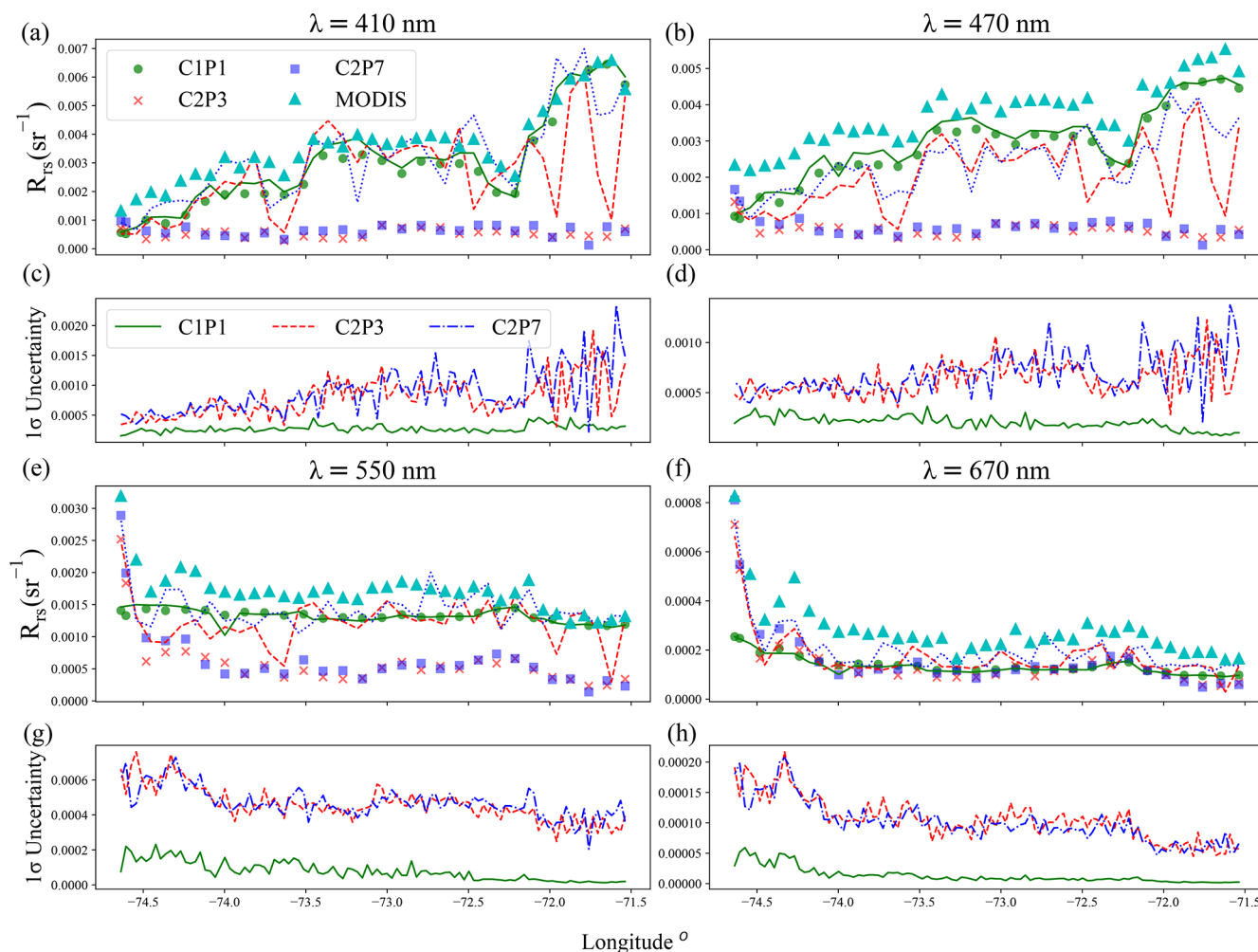


Figure 12. NAAMES-Open: the comparison of the RSP-retrieved spectral $R_{rs}(\lambda)$ across the open ocean with MODIS $R_{rs}(\lambda)$ product and uncertainty. Results are shown for the retrievals under the three bio-optical models C1P1, C2P3 and C2P7 at 410, 469, 554 and 670 nm for averaged retrievals. The lines (C1P1 – solid, C2P3 – dashed, C2P7 – dotted) indicate the retrievals obtained for the χ^2_{\min} case. The markers show the average retrieval. The uncertainty plots show the 1σ uncertainty for averaged retrievals. Data are given with respect to the longitude of the location. The coast is to the left-hand side of the plots.

6 Conclusions

In this paper, we have evaluated the performance of the MAPOL joint retrieval algorithm using three bio-optical models. The RSP measurements from different field campaigns covering different water types are used. The retrieval performance evaluation is based on the magnitude of the cost function values (χ^2), the spread of the retrieval cost function distribution, the validity of retrieved AOD, and $R_{rs}(\lambda)$ values and their respective uncertainty analysis. The three bio-optical models include C1P1, a single-parameter Case I water model, and C2P3 and C2P7, which are multi-parameter Case II bio-optical models. Three cases, ACEPOL-Mix, NAAMES-Costa and NAAMES-Open, were selected based on their location and water turbidity observed with respect to $[Chl\ a]$ derived from the NASA OBP algorithm

with MODIS measurements. NAAMES-Coastal covers highly turbid water, ACEPOL-Mix covers highly turbid and relatively clear water, and NAAMES-Open covers open clear water. The retrieved AOD was validated against that from HSRL-2 (ACEPOL-Coastal) and/or MODIS, and $R_{rs}(\lambda)$ was compared against that from MODIS. The MODIS $R_{rs}(\lambda)$ over highly turbid water shows negative values for shorter wavelengths (410 and 470 nm) that, hence, cannot be used as a validation dataset. On the other hand, the MODIS data products are used to perform sanity checks of the RSP-based MAPOL retrievals.

We evaluated the spread of the retrieval cost function distribution from the ensemble retrievals with the three bio-optical models. The C1P1 model showed narrow χ^2 distributions regardless of the type of water present or the magnitude of χ^2_{\min} values. This makes the retrieval uncertainty

from the C1P1 model smaller, even though the model cannot accurately represent a particular water type (large cost function values). Therefore convergence has to be ensured before the uncertainty evaluation, since the use of cost function distribution alone to study the retrieval uncertainties can be misleading. The C2P3 and C2P7 models showed the widest cost function distributions over open water, with χ_{\min}^2 comparable to that of C1P1. C2P3 and C2P7 showed narrow χ^2 distributions over moderately to highly turbid water with small χ^2 values. These observations implied the ability of the retrievals based on multi-parameter bio-optical models to converge near the global minimum over different water.

We also observed that the retrieval accuracies of AOD and $R_{rs}(\lambda)$ are directly related to the choice of the bio-optical model (single parameter or multi-parameter) in the retrieval. The $R_{rs}(\lambda)$ retrieval is significantly affected. The C1P1 model shows good retrieval performances only over relatively clear water ($[Chl\ a] < 3\text{ mg m}^{-3}$). The results suggested that the multi-parameter models C2P3 and C2P7 are better at representing turbid coastal water. The C2P3 and C2P7 models also have the potential to accurately represent clear open water (NAAMES-Open) in joint retrieval algorithms but with a conscientious interpretation of their χ^2 distributions. The C2P3 and C2P7 models tend to converge to local minima, and the extensive spread of χ^2 values diminishes the ability of multi-parameter models to retrieve clear water accurately and makes the interpretation of the retrieval results difficult. Therefore, it is preferred to develop screening algorithms to divide open and coastal water before performing MAP retrievals.

Similar to the SAA-based $R_{rs}(\lambda)$ inversions (Hannadige et al., 2023), multi-parameter models (C2P3 and C2P7) perform equally well when used with joint retrieval algorithms and airborne MAP measurements. The C2P3 model is more computationally efficient than the C2P7 model, as fewer free parameters lead to significantly less processing time and more stable retrieval performances.

Data availability. The data files for RSP and HSRL-2 used in this study are listed below. The RSP and HSRL-2 data are available from the ACEPOL data portal (<https://doi.org/110.5067/SUBORBITAL/ACEPOL2017/DATA001>; ACEPOL Science Team, 2017) and NAAMES data archived at the NASA Atmospheric Science Data Center (ASDC; <https://doi.org/10.5067/SUBORBITAL/NAAMES/DATA001>; NAAMES Science Team, 2017).

- ACEPOL-Mix (7 November 2017):
RSP: RSP2-ER2_L1C-RSPCOL-CollocatedRadiances_20171107T201415Z_V003-20210305T085047Z.h5
HSRL-2 : ACEPOL-HSRL2_ER2_20171107_R3.h5
- NAAMES-Coastal (4 November 2015):
RSP: RSP1-C130_L1C-RSPCOL-CollocatedRadiances_20151104T182046Z_V003-20210728T201227Z.h5

- NAAMES-Open (4 November 2015):
RSP: RSP1-C130_L1C-RSPCOL-CollocatedRadiances_20151104T173447Z_V003-20210728T201253Z.h5

Author contributions. NH formulated the methodology and software used in this paper; performed the formal analysis, investigation, data curation and visualization given in this paper; and wrote the original paper. PWZ formulated the original concept for this study. MG and PWZ developed the MAPOL retrieval algorithm. YH contributed to the development of the radiative transfer forward model and advised on the retrieval algorithm design. PJW advised and contributed to the bio-optical models and ocean water properties. BC provided the RSP measurements. KK advised on the retrieval uncertainty evaluation. All authors provided advice on the methodology and participated in writing, reviewing and editing this paper.

Competing interests. The contact author has declared that none of the authors has any competing interests.

Disclaimer. Publisher's note: Copernicus Publications remains neutral with regard to jurisdictional claims made in the text, published maps, institutional affiliations, or any other geographical representation in this paper. While Copernicus Publications makes every effort to include appropriate place names, the final responsibility lies with the authors.

Acknowledgements. The authors would like to thank the ACEPOL and NAAMES teams for conducting the field campaigns and providing the data.

The hardware used in the computational studies is part of the UMBC High Performance Computing Facility (HPCF). The facility is supported by the U.S. National Science Foundation through the MRI program and the SCREMS program, with additional substantial support from the University of Maryland, Baltimore County (UMBC). See <https://hpcf.umbc.edu/> (last access: 15 January 2023) for more information on HPCF and the projects using its resources.

Financial support. This research has been supported by the National Aeronautics and Space Administration (grant no. 80NSSC20M0227) and the Goddard Earth Sciences Technology and Research (GESTAR) II Graduate Fellowship.

Review statement. This paper was edited by Alexander Kokhanovsky and reviewed by two anonymous referees.

References

- ACEPOL Science Team: RSP and HSRL-2 data, NASA Atmospheric Science Data Center (ASDC) [data set], <https://doi.org/10.5067/SUBORBITAL/ACEPOL2017/DATA001>, 2017.

- Ahmad, Z., Franz, B. A., McClain, C. R., Kwiatkowska, E. J., Werdell, J., Shettle, E. P., and Holben, B. N.: New aerosol models for the retrieval of aerosol optical thickness and normalized water-leaving radiances from the SeaWiFS and MODIS sensors over coastal regions and open oceans, *Appl. Optics*, 49, 5545–5560, 2010.
- Bailey, S. W., Franz, B. A., and Werdell, P. J.: Estimation of near-infrared water-leaving reflectance for satellite ocean color data processing, *Opt. Express*, 18, 7521–7527, <https://doi.org/10.1364/OE.18.007521>, 2010.
- Behrenfeld, M. J., Moore, R. H., Hostetler, C. A., Graff, J., Gaube, P., Russell, L. M., Chen, G., Doney, S. C., Giovannoni, S., Liu, H., Proctor, C., Bolaños, L. M., Baetge, N., Davie-Martin, C., Westberry, T. K., Bates, T. S., Bell, T. G., Bidle, K. D., Boss, E. S., Brooks, S. D., Cairns, B., Carlson, C., Halsey, K., Harvey, E. L., Hu, C., Karp-Boss, L., Kleb, M., Menden-Deuer, S., Morison, F., Quinn, P. K., Scarino, A. J., Anderson, B., Chowdhary, J., Crosbie, E., Ferrare, R., Hair, J. W., Hu, Y., Janz, S., Redemann, J., Saltzman, E., Shook, M., Siegel, D. A., Wisthaler, A., Martin, M. Y., and Ziemba, L.: The North Atlantic Aerosol and Marine Ecosystem Study (NAAMES): Science Motive and Mission Overview, *Frontiers in Marine Science*, 6, 122, <https://doi.org/10.3389/fmars.2019.00122>, 2019.
- Boucher, O., Randall, D., Artaxo, P., Bretherton, C., Feingold, G., Forster, P., Kerminen, V.-M., Kondo, Y., Liao, H., Lohmann, U., Artaxo, P., Bretherton, C., Feingold, G., Forster, P., Kerminen, V.-M., Kondo, Y., Liao, H., Lohmann, U., Philip Rasch, P., Satheesh, S. K., Sherwood, S., Stevens, B., and Zhang, X.-Y.: Clouds and aerosols, in: *Climate change 2013: the physical science basis. Contribution of Working Group I to the Fifth Assessment Report of the Intergovernmental Panel on Climate Change*, Cambridge University Press, 571–657, <https://doi.org/10.1017/CBO9781107415324.016>, 2013.
- Bricaud, A., Morel, A., Babin, M., Allali, K., and Claustre, H.: Variations of light absorption by suspended particles with chlorophyll a concentration in oceanic (case 1) waters: Analysis and implications for bio-optical models, *J. Geophys. Res.-Oceans*, 103, 31033–31044, <https://doi.org/10.1029/98JC02712>, 1998.
- Burton, S. P., Ferrare, R. A., Vaughan, M. A., Omar, A. H., Rogers, R. R., Hostetler, C. A., and Hair, J. W.: Aerosol classification from airborne HSRL and comparisons with the CALIPSO vertical feature mask, *Atmos. Meas. Tech.*, 6, 1397–1412, <https://doi.org/10.5194/amt-6-1397-2013>, 2013.
- Cael, B., Bisson, K., Boss, E., and Erickson, Z. K.: How many independent quantities can be extracted from ocean color?, *Limnology and Oceanography Letters*, 8, 603–610, <https://doi.org/10.1002/lo12.10319>, 2023.
- Cairns, B., Russell, E. E., LaVeigne, J. D., and Tennant, P. M. W.: Research scanning polarimeter and airborne usage for remote sensing of aerosols, in: *Polarization Science and Remote Sensing*, edited by: Shaw, J. A. and Tyo, J. S., International Society for Optics and Photonics, SPIE, 5158, 33–44, <https://doi.org/10.1117/12.518320>, 2003.
- Chami, M., Shybanov, E., Churilova, T., Khomenko, G., Lee, M.-G., Martynov, O., Berseneva, G., and Korotaev, G.: Optical properties of the particles in the Crimea coastal waters (Black Sea), *J. Geophys. Res.-Oceans*, 110, C11020, <https://doi.org/10.1029/2005JC003008>, 2005.
- Chowdhary, J., Cairns, B., Mishchenko, M., and Travis, L.: Retrieval of aerosol properties over the ocean using multispectral and multiangle photopolarimetric measurements from the Research Scanning Polarimeter, *Geophys. Res. Lett.*, 28, 243–246, 2001.
- Chowdhary, J., Cairns, B., Mishchenko, M. I., Hobbs, P. V., Cota, G. F., Redemann, J., Rutledge, K., Holben, B. N., and Russell, E.: Retrieval of aerosol scattering and absorption properties from photopolarimetric observations over the ocean during the CLAMS experiment, *J. Atmos. Sci.*, 62, 1093–1117, 2005.
- Chowdhary, J., Cairns, B., Waquet, F., Knobelspiesse, K., Ottaviani, M., Redemann, J., Travis, L., and Mishchenko, M.: Sensitivity of multiangle, multispectral polarimetric remote sensing over open oceans to water-leaving radiance: Analyses of RSP data acquired during the MILAGRO campaign, *Remote Sens. Environ.*, 118, 284–308, 2012.
- Cox, C. and Munk, W.: Measurement of the Roughness of the Sea Surface from Photographs of the Sun's Glitter, *J. Opt. Soc. Am.*, 44, 838–850, <https://doi.org/10.1364/JOSA.44.000838>, 1954.
- de Almeida, D. C., Koepke, P., and Shettle, E. P.: *Atmospheric Aerosols Global Climatology and Radiative Characteristics*, Hampton, VA, USA, A. Deepak, 561 pp., ISBN: 0937194220, 1991.
- Deschamps, P.-Y., Bréon, F.-M., Leroy, M., Podaire, A., Bricaud, A., Buriez, J.-C., and Seze, G.: The POLDER mission: Instrument characteristics and scientific objectives, *IEEE T. Geosci. Remote. Char.*, 32, 598–615, 1994.
- Diner, D. J., Xu, F., Garay, M. J., Martonchik, J. V., Rheingans, B. E., Geier, S., Davis, A., Hancock, B. R., Jovanovic, V. M., Bull, M. A., Capraro, K., Chipman, R. A., and McClain, S. C.: The Airborne Multiangle SpectroPolarimetric Imager (AirMSPI): a new tool for aerosol and cloud remote sensing, *Atmos. Meas. Tech.*, 6, 2007–2025, <https://doi.org/10.5194/amt-6-2007-2013>, 2013.
- Dubovik, O., Li, Z., Mishchenko, M. I., Tanre, D., Karol, Y., Bojkov, B., Cairns, B., Diner, D. J., Espinosa, W. R., Goloub, P., Gu, X., Hasekamp, O., Hong, J., Hou, W., Knobelspiesse, K. D., Landgraf, J., Li, L., Litvinov, P., Liu, Y., Lopatin, A., Marbach, T., Maring, H., Martins, V., Meijer, Y., Milinevsky, G., Mukai, S., Parol, F., Qiao, Y., Remer, L., Rietjens, J., Sano, I., Stammes, P., Stammes, S., Sun, X., Tabary, P., Travis, L. D., Waquet, F., Xu, F., Yan, C., and Yin, D.: Polarimetric remote sensing of atmospheric aerosols: Instruments, methodologies, results, and perspectives, *J. Quant. Spectrosc. Ra.*, 224, 474–511, <https://doi.org/10.1016/j.jqsrt.2018.11.024>, 2019.
- Fan, Y., Li, W., Chen, N., Ahn, J.-H., Park, Y.-J., Kratzer, S., Schroeder, T., Ishizaka, J., Chang, R., and Stammes, K.: OC-SMART: A machine learning based data analysis platform for satellite ocean color sensors, *Remote Sens. Environ.*, 253, 112236, <https://doi.org/10.1016/j.rse.2020.112236>, 2021.
- Fougnie, B., Marbach, T., Lacan, A., Lang, R., Schlüssel, P., Poli, G., Munro, R., and Couto, A. B.: The multi-viewing multi-channel multi-polarisation imager – Overview of the 3MI polarimetric mission for aerosol and cloud characterization, *J. Quant. Spectrosc. Ra.*, 219, 23–32, <https://doi.org/10.1016/j.jqsrt.2018.07.008>, 2018.
- Fournier, G. R. and Forand, J. L.: Analytic phase function for ocean water, *SPIE*, 2258, 194–201, <https://doi.org/10.1117/12.190063>, 1994.

- Frouin, R. J., Franz, B. A., Ibrahim, A., Knobelspiesse, K., Ahmad, Z., Cairns, B., Chowdhary, J., Dierssen, H. M., Tan, J., Dubovik, O., Huang, X., Davis, A. B., Kalashnikova, O., Thompson, D. R., Remer, L. A., Boss, E., Coddington, O., Deschamps, P.-Y., Gao, B.-C., Gross, L., Hasekamp, O., Omar, A., Pelletier, B., Ramon, D., Steinmetz, F., and Zhai, P.-W.: Atmospheric Correction of Satellite Ocean-Color Imagery During the PACE Era, *Front. Earth Sci.*, 7, 145, <https://doi.org/10.3389/feart.2019.00145>, 2019.
- Gao, M., Zhai, P.-W., Franz, B., Hu, Y., Knobelspiesse, K., Werdell, P. J., Ibrahim, A., Xu, F., and Cairns, B.: Retrieval of aerosol properties and water-leaving reflectance from multi-angular polarimetric measurements over coastal waters, *Opt. Express*, 26, 8968–8989, 2018.
- Gao, M., Zhai, P.-W., Franz, B. A., Hu, Y., Knobelspiesse, K., Werdell, P. J., Ibrahim, A., Cairns, B., and Chase, A.: Inversion of multiangular polarimetric measurements over open and coastal ocean waters: a joint retrieval algorithm for aerosol and water-leaving radiance properties, *Atmos. Meas. Tech.*, 12, 3921–3941, <https://doi.org/10.5194/amt-12-3921-2019>, 2019.
- Gao, M., Zhai, P.-W., Franz, B. A., Knobelspiesse, K., Ibrahim, A., Cairns, B., Craig, S. E., Fu, G., Hasekamp, O., Hu, Y., and Werdell, P. J.: Inversion of multiangular polarimetric measurements from the ACEPOL campaign: an application of improving aerosol property and hyperspectral ocean color retrievals, *Atmos. Meas. Tech.*, 13, 3939–3956, <https://doi.org/10.5194/amt-13-3939-2020>, 2020.
- Gao, M., Franz, B. A., Knobelspiesse, K., Zhai, P.-W., Martins, V., Burton, S., Cairns, B., Ferrare, R., Gales, J., Hasekamp, O., Hu, Y., Ibrahim, A., McBride, B., Puthukkudy, A., Werdell, P. J., and Xu, X.: Efficient multi-angle polarimetric inversion of aerosols and ocean color powered by a deep neural network forward model, *Atmos. Meas. Tech.*, 14, 4083–4110, <https://doi.org/10.5194/amt-14-4083-2021>, 2021.
- Gao, M., Knobelspiesse, K., Franz, B. A., Zhai, P.-W., Cairns, B., Xu, X., and Martins, J. V.: The impact and estimation of uncertainty correlation for multi-angle polarimetric remote sensing of aerosols and ocean color, *Atmos. Meas. Tech.*, 16, 2067–2087, <https://doi.org/10.5194/amt-16-2067-2023>, 2023.
- Gordon, H. R.: Evolution of Ocean Color Atmospheric Correction: 1970–2005, *Remote Sensing*, 13, 5051, <https://doi.org/10.3390/rs13245051>, 2021.
- Gordon, H. R. and Wang, M.: Retrieval of water-leaving radiance and aerosol optical thickness over the oceans with SeaWiFS: a preliminary algorithm, *Appl. Optics*, 33, 443–452, <https://doi.org/10.1364/AO.33.000443>, 1994.
- Hannadige, N. K., Zhai, P.-W., Gao, M., Franz, B. A., Hu, Y., Knobelspiesse, K., Werdell, P. J., Ibrahim, A., Cairns, B., and Hasekamp, O. P.: Atmospheric correction over the ocean for hyperspectral radiometers using multi-angle polarimetric retrievals, *Opt. Express*, 29, 4504–4522, 2021.
- Hannadige, N. K., Zhai, P.-W., Werdell, P. J., Gao, M., Franz, B. A., Knobelspiesse, K., and Ibrahim, A.: Optimizing retrieval spaces of bio-optical models for remote sensing of ocean color, *Appl. Optics*, 62, 3299–3309, 2023.
- Hasekamp, O. P. and Landgraf, J.: Retrieval of aerosol properties over land surfaces: capabilities of multiple-viewing-angle intensity and polarization measurements, *Appl. Optics*, 46, 3332–3344, 2007.
- Hasekamp, O. P., Litvinov, P., and Butz, A.: Aerosol properties over the ocean from PARASOL multiangle photopolarimetric measurements, *J. Geophys. Res.-Atmos.*, 116, D14204, <https://doi.org/10.1029/2010JD015469>, 2011.
- He, X., Bai, Y., Pan, D., Tang, J., and Wang, D.: Atmospheric correction of satellite ocean color imagery using the ultraviolet wavelength for highly turbid waters, *Opt. Express*, 20, 20754–20770, <https://doi.org/10.1364/OE.20.020754>, 2012.
- Hu, C., Lee, Z., and Franz, B.: Chlorophyll algorithms for oligotrophic oceans: A novel approach based on three-band reflectance difference, *J. Geophys. Res.-Oceans*, 117, C01011, <https://doi.org/10.1029/2011JC007395>, 2012.
- Huot, Y., Morel, A., Twardowski, M. S., Stramski, D., and Reynolds, R. A.: Particle optical backscattering along a chlorophyll gradient in the upper layer of the eastern South Pacific Ocean, *Biogeosciences*, 5, 495–507, <https://doi.org/10.5194/bg-5-495-2008>, 2008.
- Ibrahim, A., Franz, B. A., Ahmad, Z., and Bailey, S. W.: Multiband Atmospheric Correction Algorithm for Ocean Color Retrievals, *Front. Earth Sci.*, 7, 116, <https://doi.org/10.3389/feart.2019.00116>, 2019.
- IOCCG: Remote Sensing of Ocean Colour in Coastal, and Other Optically-Complex, Waters, in: Reports of the International Ocean Colour Coordinating Group, IOCCG, Dartmouth, Canada, Vol. 3, <https://doi.org/10.25607/OBP-95>, 2000.
- IOCCG: Remote Sensing of Inherent Optical Properties: Fundamentals, Tests of Algorithms, and Application, in: Reports of the International Ocean Colour Coordinating Group, IOCCG, Dartmouth, Canada, Vol. 5, <https://doi.org/10.25607/OBP-96>, 2006.
- IOCCG: Atmospheric Correction for Remotely-Sensed Ocean-Colour Products, in: Reports of the International Ocean Colour Coordinating Group, IOCCG, Dartmouth, Canada, Vol. 10, <https://doi.org/10.25607/OBP-101>, 2010.
- IOCCG: Phytoplankton Functional Types from Space, in: Reports of the International Ocean Colour Coordinating Group, IOCCG, Dartmouth, Canada, Vol. 15, <https://doi.org/10.25607/OBP-106>, 2014.
- Jonasz, M.: Light scattering by particles in water theoretical and experimental foundations, Academic Press, London, UK, ISBN 1-281-11914-8, 2007.
- Knobelspiesse, K., Cairns, B., Mishchenko, M., Chowdhary, J., Tsigaridis, K., van Dienenhoven, B., Martin, W., Ottaviani, M., and Alexandrov, M.: Analysis of fine-mode aerosol retrieval capabilities by different passive remote sensing instrument designs, *Opt. Express*, 20, 21457–21484, 2012.
- Knobelspiesse, K., Tan, Q., Bruegge, C., Cairns, B., Chowdhary, J., van Dienenhoven, B., Diner, D., Ferrare, R., van Harten, G., Jovanovic, V., Ottaviani, M., Redemann, J., Seidel, F., and Sinclair, K.: Intercomparison of airborne multi-angle polarimeter observations from the Polarimeter Definition Experiment, *Appl. Optics*, 58, 650–669, <https://doi.org/10.1364/AO.58.000650>, 2019.
- Knobelspiesse, K., Barbosa, H. M. J., Bradley, C., Bruegge, C., Cairns, B., Chen, G., Chowdhary, J., Cook, A., Di Noia, A., van Dienenhoven, B., Diner, D. J., Ferrare, R., Fu, G., Gao, M., Garay, M., Hair, J., Harper, D., van Harten, G., Hasekamp, O., Helmlinger, M., Hostetler, C., Kalashnikova, O., Kupchock, A., Longo De Freitas, K., Maring, H., Martins, J. V., McBride, B., McGill, M., Norlin, K., Puthukkudy, A., Rheingans, B., Riet-

- jens, J., Seidel, F. C., da Silva, A., Smit, M., Stamnes, S., Tan, Q., Val, S., Wasilewski, A., Xu, F., Xu, X., and Yorks, J.: The Aerosol Characterization from Polarimeter and Lidar (ACEPOL) airborne field campaign, *Earth Syst. Sci. Data*, 12, 2183–2208, <https://doi.org/10.5194/essd-12-2183-2020>, 2020.
- Kokhanovsky, A. A.: Parameterization of the Mueller matrix of oceanic waters, *J. Geophys. Res.-Oceans*, 108, 3175, <https://doi.org/10.1029/2001JC001222>, 2003.
- Li, Z., Guo, J., Ding, A., Liao, H., Liu, J., Sun, Y., Wang, T., Xue, H., Zhang, H., and Zhu, B.: Aerosol and boundary-layer interactions and impact on air quality, *Natl. Sci. Rev.*, 4, 810–833, <https://doi.org/10.1093/nsr/nwx117>, 2017.
- Mishchenko, M. I. and Travis, L. D.: Satellite retrieval of aerosol properties over the ocean using polarization as well as intensity of reflected sunlight, *J. Geophys. Res.-Atmos.*, 102, 16989–17013, 1997.
- Mishchenko, M. I., Cairns, B., Hansen, J. E., Travis, L. D., Burg, R., Kaufman, Y. J., Martins, J. V., and Shettle, E. P.: Monitoring of aerosol forcing of climate from space: analysis of measurement requirements, *J. Quant. Spectrosc. Ra.*, 88, 149–161, 2004.
- Mobley, C., Werdell, J., Franz, B., Ahmad, Z., and Bailey, S.: Atmospheric Correction for Satellite Ocean Color Radiometry, National Aeronautics and Space Administration, Tech. Rep. No. GSFC-E-DAA-TN35509, ID 20160011399, <https://doi.org/10.13140/RG.2.2.23016.78081>, 2016.
- Mobley, C. D., Gentili, B., Gordon, H. R., Jin, Z., Kattawar, G. W., Morel, A., Reinersman, P., Stamnes, K., and Stavn, R. H.: Comparison of numerical models for computing underwater light fields, *Appl. Optics*, 32, 7484–7504, <https://doi.org/10.1364/AO.32.007484>, 1993.
- NAAMES Science Team: NAAMES (North Atlantic Aerosols and Marine Ecosystems Study) data, NASA Atmospheric Science Data Center (ASDC) [data set], <https://doi.org/10.5067/SUBORBITAL/NAAMES/DATA001>, 2017.
- Remer, L. A., Kaufman, Y. J., Tanré, D., Mattoo, S., Chu, D. A., Martins, J. V., Li, R.-R., Ichoku, C., Levy, R. C., Kleidman, R. G., Eck, T. F., Vermote, E., and Holben, B. N.: The MODIS Aerosol Algorithm, Products, and Validation, *J. Atmos. Sci.*, 62, 947–973, <https://doi.org/10.1175/JAS3385.1>, 2005.
- Remer, L. A., Davis, A. B., Mattoo, S., Levy, R. C., Kalashnikova, O. V., Coddington, O., Chowdhary, J., Knobelspiesse, K., Xu, X., Ahmad, Z., Boss, E., Cairns, B., Dierssen, H. M., Diner, D. J., Franz, B., Frouin, R., Gao, B.-C., Ibrahim, A., Martins, J. V., Omar, A. H., Torres, O., Xu, F., and Zhai, P.-W.: Retrieving aerosol characteristics from the PACE mission, Part 1: Ocean Color Instrument, *Front. Earth Sci.*, 7, 152, <https://doi.org/10.3389/feart.2019.00152>, 2019a.
- Remer, L. A., Knobelspiesse, K., Zhai, P.-W., Xu, F., Kalashnikova, O. V., Chowdhary, J., Hasekamp, O., Dubovik, O., Wu, L., Ahmad, Z., Boss, E., Cairns, B., Coddington, O., Davis, A. B., Dierssen, H. M., Diner, D. J., Franz, B., Frouin, R., Gao, B.-C., Ibrahim, A., Levy, R. C., Martins, J. V., Omar, A. H., and Torres, O.: Retrieving aerosol characteristics from the PACE mission, Part 2: multi-angle and polarimetry, *Frontiers in Environmental Science*, 7, 94, <https://doi.org/10.3389/fenvs.2019.00094>, 2019b.
- Roesler, C. S., Perry, M. J., and Carder, K. L.: Modeling in situ phytoplankton absorption from total absorption spectra in productive inland marine waters, *Limnol. Oceanogr.*, 34, 1510–1523, 1989.
- Sayer, A. M., Hsu, N., Bettenhausen, C., Lee, J., Redemann, J., Schmid, B., and Shinozuka, Y.: Extending “Deep Blue” aerosol retrieval coverage to cases of absorbing aerosols above clouds: Sensitivity analysis and first case studies, *J. Geophys. Res.-Atmos.*, 121, 4830–4854, 2016.
- Shettle, E. P. and Fenn, R. W.: Models for the aerosols of the lower atmosphere and the effects of humidity variations on their optical properties, Environmental Research Papers, Air Force Geophysics Lab., Hanscom AFB, MA, Optical Physics Div, AFGL-TR-79-0214, 1979.
- Smit, M., Rietjens, J., di Noia, A., Hasekamp, O., Laauwen, W., Cairns, B., van Diedenhoven, B., and Wasilewski, A.: In-flight validation of SPEX airborne spectropolarimeter onboard NASA’s research aircraft ER-2, 22 pp., <https://doi.org/10.1117/12.2535942>, 2019.
- Stamnes, S., Hostetler, C., Ferrare, R., Burton, S., Liu, X., Hair, J., Hu, Y., Wasilewski, A., Martin, W., Van Diedenhoven, B., Chowdhary, J., Cetinić, I., Berg, L. K., Stamnes, K., and Cairns, B.: Simultaneous polarimeter retrievals of microphysical aerosol and ocean color parameters from the “MAPP” algorithm with comparison to high-spectral-resolution lidar aerosol and ocean products, *Appl. Optics*, 57, 2394–2413, 2018.
- Utry, N., Ajtai, T., Pintér, M., Bozóki, Z., and Szabó, G.: Wavelength-dependent optical absorption properties of artificial and atmospheric aerosol measured by a multi-wavelength photoacoustic spectrometer, *Int. J. Thermophys.*, 35, 2246–2258, 2014.
- Van Harten, G., Davis, A., Diner, D. J., Bailey, T., Brageot, E., Bruegge, C., Hancock, B., Hutchinson, L., Manatt, K., Patel, S., Pearson, J., Rheingans, B., Sandhu, J., Shelton, J., Steffy, A., Warner, D., and Werne, T.: Polarimetric calibration of the multi-angle imager for aerosols (MAIA), in: *Sensors, Systems, and Next-Generation Satellites XXV*, SPIE, 11858, 79–97, 2021.
- Voss, K. J. and Fry, E. S.: Measurement of the Mueller matrix for ocean water, *Appl. Optics*, 23, 4427–4439, <https://doi.org/10.1364/AO.23.004427>, 1984.
- Werdell, P. J., Franz, B. A., Bailey, S. W., Feldman, G. C., Boss, E., Brando, V. E., Dowell, M., Hirata, T., Lavender, S. J., Lee, Z., Loisel, H., Maritorea, S., Mélin, F., Moore, T. S., Smyth, T. J., Antoine, D., Emmanuel Devred, E., d’Andon, O. H. F., and Mangin, A.: Generalized ocean color inversion model for retrieving marine inherent optical properties, *Appl. Optics*, 52, 2019–2037, 2013.
- Werdell, P. J., Behrenfeld, M. J., Bontempi, P. S., Boss, E., Cairns, B., Davis, G. T., Franz, B. A., Gliese, U. B., Gorman, E. T., Hasekamp, O., Knobelspiesse, K. D., Mannino, A., Martins, J. V., McClain, C. R., Meister, G., and Remer, L. A.: The Plankton, Aerosol, Cloud, Ocean Ecosystem Mission: Status, Science, Advances, *B. Am. Meteorol. Soc.*, 100, 1775–1794, <https://doi.org/10.1175/BAMS-D-18-0056.1>, 2019.
- Whitmire, A. L., Boss, E., Cowles, T. J., and Pegau, W. S.: Spectral variability of the particulate backscattering ratio, *Opt. Express*, 15, 7019–7031, 2007.

- Xu, F., Dubovik, O., Zhai, P.-W., Diner, D. J., Kalashnikova, O. V., Seidel, F. C., Litvinov, P., Bovchaliuk, A., Garay, M. J., van Harten, G., and Davis, A. B.: Joint retrieval of aerosol and water-leaving radiance from multispectral, multiangular and polarimetric measurements over ocean, *Atmos. Meas. Tech.*, 9, 2877–2907, <https://doi.org/10.5194/amt-9-2877-2016>, 2016.
- Zhai, P.-W., Hu, Y., Trepte, C. R., and Lucker, P. L.: A vector radiative transfer model for coupled atmosphere and ocean systems based on successive order of scattering method, *Opt. Express*, 17, 2057–2079, <https://doi.org/10.1364/OE.17.002057>, 2009.
- Zhai, P.-W., Hu, Y., Chowdhary, J., Trepte, C. R., Lucker, P. L., and Josset, D. B.: A vector radiative transfer model for coupled atmosphere and ocean systems with a rough interface, *J. Quant. Spectrosc. Ra.*, 111, 1025–1040, <https://doi.org/10.1016/j.jqsrt.2009.12.005>, 2010.
- Zhai, P.-W., Hu, Y., Winker, D. M., Franz, B. A., and Boss, E.: Contribution of Raman scattering to polarized radiation field in ocean waters, *Opt. Express*, 23, 23582–23596, <https://doi.org/10.1364/OE.23.023582>, 2015.
- Zhai, P.-W., Knobelspiesse, K., Ibrahim, A., Franz, B. A., Hu, Y., Gao, M., and Frouin, R.: Water-leaving contribution to polarized radiation field over ocean, *Opt. Express*, 25, A689–A708, <https://doi.org/10.1364/OE.25.00A689>, 2017.
- Zibordi, G., Mélin, F., Berthon, J.-F., Holben, B., Slutsker, I., Giles, D., D’Alimonte, D., Vandemark, D., Feng, H., Schuster, G., Fabbri, B. E., Kaitala, S., and Seppälä, J.: AERONET-OC: A Network for the Validation of Ocean Color Primary Products, *J. Atmos. Ocean. Tech.*, 26, 1634–1651, <https://doi.org/10.1175/2009JTECHO654.1>, 2009.